JOURNAL OF GEOPHYSICAL RESEARCH, VOL. 97, NO. D11, PAGES 11,487–11,512, JULY 20, 1992

A Study of Broadband Parameterizations of the Solar Radiative Interactions With Water Vapor and Water Drops

V. RAMASWAMY

Atmospheric and Oceanic Sciences Program, Princeton University, Princeton, New Jersey

S. M. FREIDENREICH

NOAA Geophysical Fluid Dynamics Laboratory, Princeton, New Jersey

Reference radiative transfer solutions in the near-infrared spectrum, which account for the spectral absorption characteristics of the water vapor molecule and the absorbing-scattering features of water drops, are employed to investigate and develop broadband treatments of solar water vapor absorption and cloud radiative effects. The conceptually simple and widely used Lacis-Hansen parameterization for solar water vapor absorption is modified so as to yield excellent agreement in the clear sky heating rates. The problem of single cloud decks over a nonreflecting surface is used to highlight the factors involved in the development of broadband overcast sky parameterizations. Three factors warrant considerable attention: (1) the manner in which the spectrally dependent drop single-scattering values are used to obtain the broadband cloud radiative properties, (2) the effect of the spectral attenuation by the vapor above the cloud on the determination of the broadband drop reflection and transmission, and (3) the broadband treatment of the spectrally dependent absorption due to drops and vapor inside the cloud. The solar flux convergence in clouds is very sensitive to all these considerations. Ignoring effect 2 tends to overestimate the cloud heating, particularly for low clouds, while a poor treatment of effect 3 leads to an underestimate. A new parameterization that accounts for the aforementioned considerations is accurate to within ~30% over a wide range of overcast sky conditions, including solar zenith angles and cloud characteristics (altitudes, drop models, optical depths, and geometrical thicknesses), with the largest inaccuracies occurring for geometrically thick, extended cloud systems containing large amounts of vapor. Broadband methods that treat improperly one or more of the above considerations can yield substantially higher errors (>35%) for some overcast sky conditions while having better agreements over limited portions of the parameter range. For example, a technique that considers effect 3 but ignores effect 2 yields a partial compensation of errors of opposite sign, such that the resulting inaccuracy for geometrically thick clouds can be less than 20%. In contrast to the marked sensitivity of the cloud heating rates, the maximum relative errors in the reflected flux at the top of the overcast atmosphere and the transmitted flux at the surface do not vary appreciably under the various broadband treatments; with the new parameterization, the relative errors are less than 15%. In applying the broadband concept to overcast atmospheres with multiple cloud decks, there are cases when the errors can be larger than stated above. Hence a general use of broadband methods in weather prediction and climate models (e.g., general circulation models) should be accompanied by a realization of the potential inaccuracies that can occur for specific overcast sky cases.

INTRODUCTION

The vertical disposition of the solar radiation within the Earth's inhomogeneous atmosphere due to interactions with the vapor and condensed forms of water constitutes a significant component of the energy budget of the surface-atmosphere system. Approximately 71% of the solar irradiance is contained in the frequency interval 0–18,000 cm^{-1} (i.e., wavelengths longer than 0.55 μm), which includes the near-infrared spectrum. This interval is particularly interesting, as both absorption (water vapor and drops) and scattering (drops only) become important here. For example, line-by-line (LBL) studies [*Ramaswamy and Freidenreich*, 1991, hereinafter RF] show that at a solar zenith angle of 30°, a lower tropospheric cloud of optical depth ~10 can reflect a third and absorb three tenths of the solar irradiance at the top of the atmosphere in this interval. The heating rate in the cloud layers easily exceeds that due to absorption by water vapor in clear skies. Taken together, the H_2O forms constitute a major source of the tropospheric radiative convergence.

While it is easy in principle to resolve the absorbing-scattering problem with high-resolution algorithms [*Davies et al.*, 1984; *Wiscombe et al.*, 1984; RF], such schemes are computationally expensive and pose severe timing constraints when radiative fluxes and heating rates have to be performed routinely for energy budget or weather/climate studies (e.g., in general circulation models, or GCMs). This has initiated several quests over the years to develop efficient yet accurate broadband parameterizations for the solar radiation interactions with water vapor and/or liquid water forms, dating at least as far back as *Fowle* [1915] and *Yamamoto* [1962], and continuing with the studies of *Lacis and Hansen* [1974] (hereinafter LH), *Stephens et al.* [1984], *Kratz and Cess* [1985] (hereinafter KC) and *Slingo* [1989], to name a few. The term broadband in the context of GCMs has usually implied the use of one effective spectral band to represent the radiative transfer effects over the entire near-infrared spectrum. The use of such a broad spectral interval is necessitated when the optical properties of at least one of the constituents are available only for the spectrum as a whole.

Paper number 92JD00932
0148-0227/92/92JD-00932$05.00

The parameterization of the absorbing-scattering problem involving vapor and drops involves the convolution of the spectrally dependent values of three different physical entities: the incoming solar irradiance, the spectral features of the water vapor molecule, and the single-scattering properties of water drops. Figure 1 illustrates the distinctly different spectral variations that occur in the solar flux at the top of the atmosphere, in the atmospheric absorption optical depth of water vapor, and in the coalbedo (absorption at each scattering event) of two typical water drop size distributions used in the Intercomparison of Radiation Codes in Climate Models (ICRCCM) project [*Fouquart et al.*, 1991].

For the absorption problem in clear (i.e., cloudless) skies, LH obtained a conceptually simple and reasonable formulation for the broadband solar absorption by water vapor (i.e., the convolution of the solar flux with the spectral features of the H_2O molecule). The study by KC presented an improved formulation for the same physical process. The expressions obtained in these two studies have been deployed in several GCM studies. However, as will be shown later, both these broadband expressions require further adjustments in order to improve their accuracy.

An accurate broadband representation of the solar interactions with drops alone also has been obtained in an economical manner [*Slingo*, 1989]. While broadband water vapor absorption expressions have a simple dependence on the vapor optical path, liquid water and effective radii seem to capture the broadband drop radiative properties adequately. In contrast, for overcast situations where both vapor and drops are present, there arise more intricate and significant dependences for the absorption and scattering processes, as will be highlighted in this paper.

In this study, high-spectral-resolution results for vapor-only and overcast (vapor and drops) skies are determined corresponding to a range of atmospheric situations. These reference results are then used in three ways: to study the quantitative dependence of the inhomogeneous radiative transfer on various parameters, to evaluate and modify (or obtain) suitable parametric fits that incorporate these dependences explicitly, and to determine the accuracy of the resulting broadband parameterizations of vapor and vapor plus drop radiative interactions for a variety of cases. While the investigations here are concerned primarily with the absorbed solar flux, the accuracies in the reflected flux at the top of the atmosphere and in the surface flux are also discussed.

Although the solar absorption-scattering problem involving H_2O has been treated in past studies usually for the 2500 to 13,000 cm^{-1} spectral regime, we consider the interval 0–18,000 cm^{-1} to be the basis of the broadband parameterization, in view of the presence of water vapor spectral lines throughout this interval in the Air Force Geophysics Laboratory (AFGL) catalog [*Rothman et al.*, 1983]. Section 2 evaluates the accuracy of the two commonly employed broadband water vapor absorption schemes and presents a modification in one of them that improves its accuracy. Section 3 describes the framework for calculations used as a reference set here to study the overcast sky transfer. Using the problem of single cloud decks above a nonreflecting surface, section 4 highlights the considerations essential for the development of broadband overcast sky formulations and discusses a parameterization approach. The application and the accuracy of this approach are discussed in section 5.

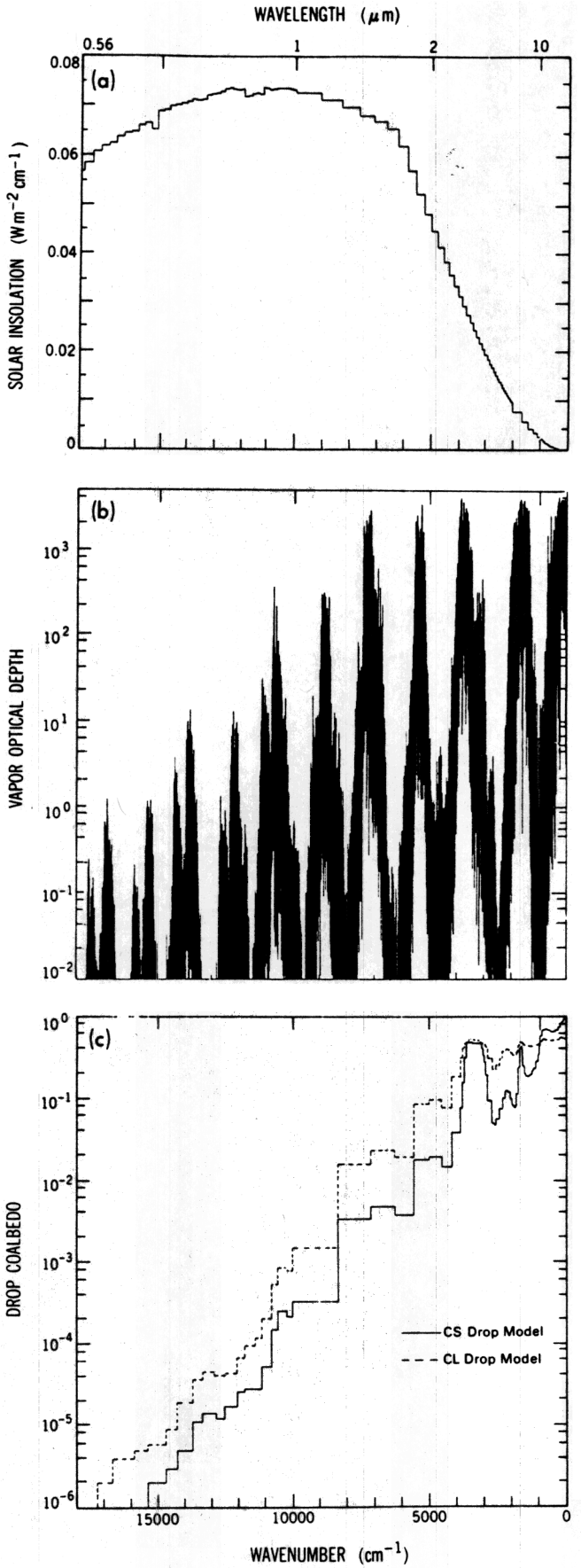

Fig. 1. Spectral variation of (*a*) the solar flux per wavenumber, (*b*) the water vapor optical depth in the midlatitude summer atmosphere [*McClatchey et al.*, 1972] and (*c*) the drop coalbedo of CS and CL drop models (see text) over the interval 0–18,000 cm^{-1}.

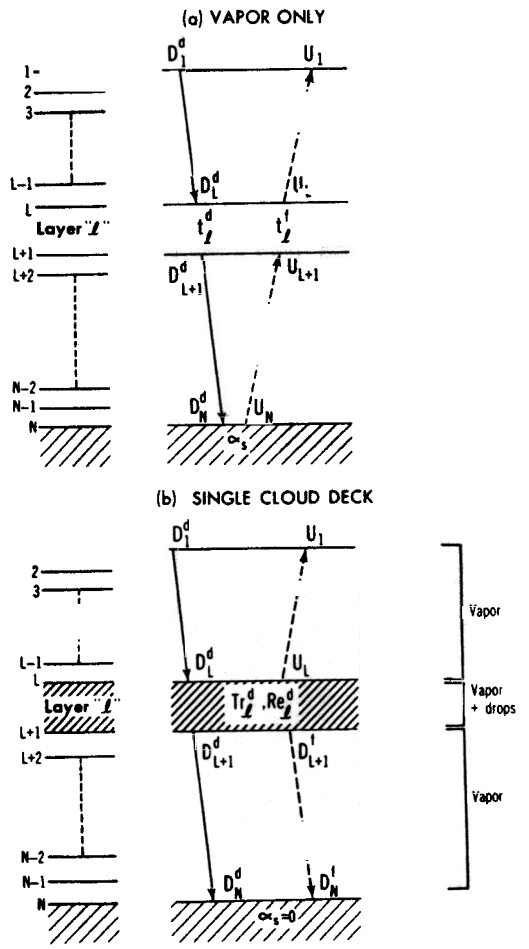

Fig. 2. Schematic of the N-level model used to obtain reference solutions for the radiative transfer problem in a vertically inhomogeneous atmosphere containing (a) water vapor only above a Lambertian surface (albedo α_s) and (b) water vapor and a single cloud deck (layer l) above a nonreflecting surface. In Figure 2a the downward beam D consists of only the direct (i.e., unscattered) component D^d, with D_1^d being the incident solar radiation at the top. In Figure 2b there is, in addition, a diffuse (i.e., radiation scattered at least once) beam D^f. U refers to the upward beam which is diffuse. Transmission due to layers containing vapor only is denoted by t, while Tr and Re denote the cloud layer transmission and reflection, respectively; the superscripts denote the layer properties with respect to the direct (d) or diffuse (f) beam.

Section 6 investigates the accuracy of various broadband overcast sky treatments that have been employed in or proposed for GCM weather prediction and climate studies. Section 7 discusses the extension of the broadband concept to arbitrary overcast atmospheres, while section 8 summarizes the principal findings of this study.

2. Water Vapor Absorption

At any monochromatic frequency (notation suppressed in this section), the total (direct + diffuse) downward solar flux at any level L (counted from top downward) in a clear atmosphere containing only water vapor (Figure 2a) is just the direct flux and is given by

$$D_L^d = F_0 \prod_{j=1}^{L-1} t_j^d \tag{1}$$

where D stands for total downward solar radiation, the superscript "d" denotes unscattered direct radiation, with $D_1^d = F_0$ being the direct downward incident solar radiation at the top of the atmosphere; t_j^d is the direct beam transmission due to water vapor in the jth layer located between levels j, $j+1$

$$t_j^d = \exp\left(-\frac{\tau_{\text{vap},j}}{\mu_0}\right) \tag{2}$$

where $\tau_{\text{vap},j}$ is the optical depth of the vapor in the layer,

$$\tau_{\text{vap},j} = \frac{q_j k_j dp_j}{g_0} \tag{3}$$

dp is the pressure thickness of the layer, q is the mixing ratio and k the absorption coefficient of the layer; g_0 is the acceleration due to gravity, and μ_0 is the cosine of the incident solar zenith angle. For a Lambertian surface with a nonzero albedo α_s, the reflection at the surface (level N) generates a diffuse beam (Figure 2a) which is isotropic. The diffuse upward flux at level L is given by

$$U_L = (\alpha_s D_N^d) \prod_{j=L}^{N-1} t_j^f \tag{4}$$

where t_j^f is the transmission of diffuse (superscript f refers to diffuse) radiation by the jth layer

$$t_j^f = 2\int_0^1 \exp\left(-\frac{\tau_{\text{vap},j}}{\mu}\right) \mu \, d\mu \tag{5}$$

the integration over the angle (μ) is evaluated using a four-point Gauss quadrature scheme. The heating rate in the lth layer, located between pressure levels P_L and P_{L+1} (see Figure 2a) is given by

$$Q_l = \frac{(g_0/c_p)(D_L^d - U_L - D_{L+1}^d + U_{L+1})}{(P_{L+1} - P_L)} \tag{6}$$

where c_p is the specific heat at constant pressure.

The determination of the near-infrared fluxes and heating rates for the different model atmospheres [*McClatchey et al.*, 1972] is carried out according to equations (1)–(6), using the LBL technique described by RF. The model atmosphere (Figure 2a) consists of fifty 20-mbar-thick layers between 0 and 1000 mbar while the lowest layer is 13 mbar thick. These computations represent the reference results for the vapor-only atmosphere and were performed for a range of zenith angles and surface albedos.

The primary need of any broadband parameterization is to obtain a simple algebraic expression that captures accurately the spectrally integrated features across the spectrum. Two parameterizations which have been used in several GCMs are due to LH and KC, respectively. Figures 3 and 4 illustrate the heating rates obtained from these two schemes and the LBL method for solar zenith angles Θ_0 of 30° and 75° in a mid-latitude summer atmosphere with a surface albedo of 0.2; the choices concerning surface albedo and angles are motivated by the ICRCCM exercises [*Fouquart et al.*, 1991]. Absolute errors in the two parameterizations with respect to the LBL results are also shown in the same figures. The main deficiency of the LH scheme, as was noted earlier by KC, is

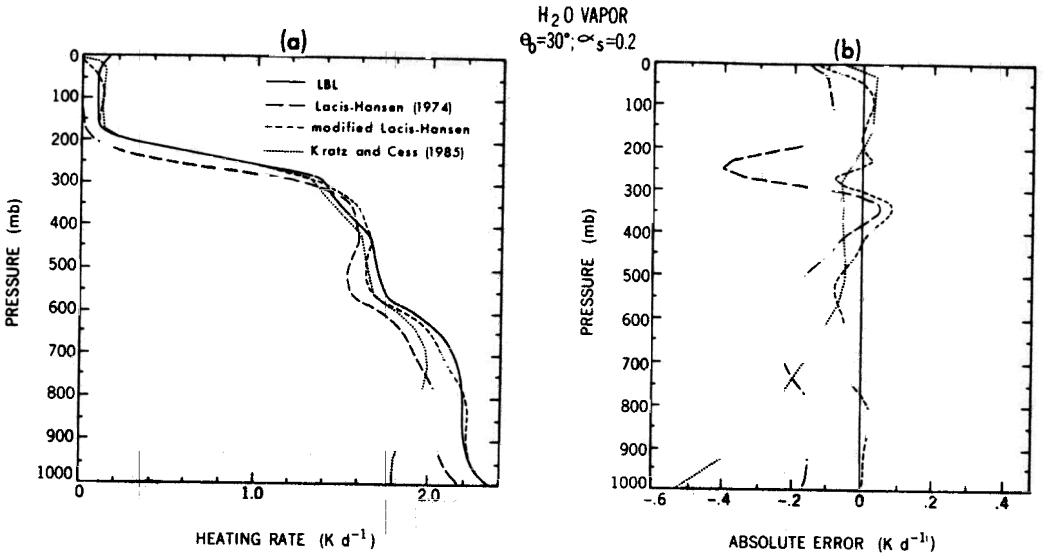

Fig. 3. Solar absorption by water vapor in a mid-latitude summer atmosphere (zenith angle $\Theta_0 = 30°$; surface albedo $\alpha_s = 0.2$). (*a*) Vertical profile of the heating rate as determined by the line-by-line (LBL) method and by three different parameterizations, including the one developed in this study (modified Lacis-Hansen). (*b*) Absolute errors due to the parameterizations with respect to the LBL result.

the underestimate occurring in the upper troposphere and the lower stratosphere. The radiative time constant for this region is large so that any heating deficit is likely to lead to a cold bias in GCM simulations. This prompted KC to develop a formulation based on a 5 cm^{-1} narrowband model that rectified the shortcomings in the upper troposphere. However, the heating predicted in the latter scheme exhibits a deficit in the middle and lower tropospheric layers. The LH scheme, too, exhibits a slight underestimate in the lower troposphere. As a result, the atmospheric absorbed flux computed by these two methods underestimates the LBL values, both for the direct and the total beam (Table 1).

In order to correct for the underestimates in the absorption, the original LH formulation for the atmospheric water vapor transmission is modified in this paper. Specifically, three more exponential-sum terms have been added to the eight listed by LH (their Table 1), resulting in 11 pseudomonochromatic intervals. Each of the three new terms has a different absorption coefficient and weight, and their introduction is accompanied by a readjustment in the weights of the eight original LH terms. The values of the new absorption coefficients and the new weights under the "modified LH scheme" are listed in Table 2. The new set of weights also account for the fact that water vapor absorption extends from 0 to 18,000 cm^{-1} (i.e., wavelengths longward of 0.55 μm).

Heating rates obtained with the modified LH scheme and its absolute errors are also shown in Figures 3 and 4 for zenith angles of 30° and 75°, respectively. The new scheme introduces errors of less than 0.1 K/d in the mid-latitude

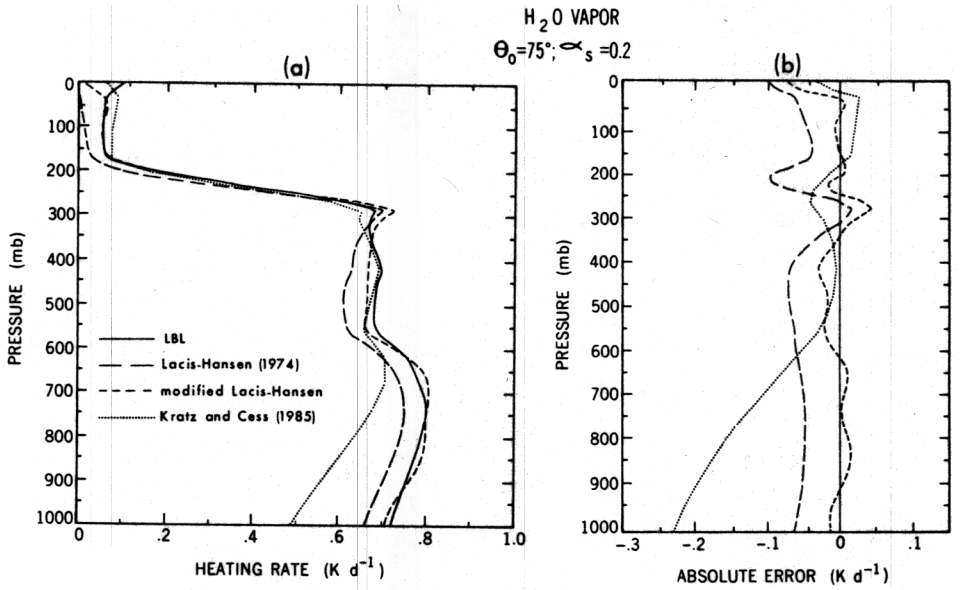

Fig. 4. Same as Figure 3, except $\Theta_0 = 75°$.

summer atmosphere. The modified LH parameterization in general improves the heating rates throughout the atmosphere, including the upper troposphere and the lower stratosphere. There is an overestimate between ~300–400 mbar in Figure 3 and ~250–350 mbar in Figure 4 which exceeds that in the original LH scheme. The heating rates for other atmospheric profiles obtained with the modified scheme also agree well with the LBL results (Figure 5); the major shortcoming occurs for the sub-Arctic winter (SAW) case where the error in the middle troposphere for $\Theta_0 = 30°$ reaches 0.16 K/d. The effects of considering different zenith angles (0°, 53°, and 75°) and a high surface albedo (0.8) are shown in Figure 6. In contrast to Figures 3 and 4, note the increase in the heating that takes place in the lower atmosphere (Figure 6*a*) due to reflection at the surface and the subsequent absorption by the water vapor in the layers immediately above the surface. Figure 6*b* illustrates the successful representation of this feature (error of ~0.1 K/d or less) by the modified parameterization.

The good simulations of the heating rates (error < 10%) and the absorbed atmospheric fluxes (error < 3%) for the conditions considered (Figures 3–6; Table 1) suggest that the modified LH scheme is an acceptable broadband treatment of the water vapor absorption. Inasmuch as only three terms are added to the original LH formulation, this retains the conceptual simplicity of the original LH scheme and results in a more accurate representation, with only a modest increase in the burden of the radiative computations. The fact that only 11 terms are needed to describe the water vapor absorption due to some 3 million discrete frequency points, as used in the LBL calculations [RF], is a very encouraging development for solar radiative parameterizations. However, this conclusion regarding the broadband approach is tempered when overcast sky conditions are considered.

3. Reference Solutions for Overcast Atmospheres

Consider a cloud consisting of a specific drop-size distribution located in layer l between levels L and $L + 1$ in a model atmosphere containing water vapor (Figure 2*b*). At any frequency ν, the total downward flux at the cloud top (level L) consists of the direct flux only, as given by (1). After traversing the cloud, a portion of the direct beam emerges as unscattered flux. The portion scattered at least once in the cloud layer is a diffuse beam, assumed to be isotropic. If the surface has a nonzero albedo or if there are other cloud decks in the atmosphere, there will be multiple reflections of both these beams. For ease in highlighting the role of vapor and drops, our focus in this study is mainly on the fundamental problem of a single cloud deck over a nonreflecting surface. In this case, the only radiation incident on the cloud is the direct beam (D_L^d). As will be shown, the task of representing the direct beam overcast sky interactions within a broadband framework by itself requires a series of careful, detailed considerations. Subsequently, we explore the consequence of extending the broadband framework to the general overcast sky problem.

TABLE 1. Solar Flux Absorbed by Water Vapor in the Mid-Latitude Summer Atmosphere According to the Line-by-Line Computations and the Lacis-Hansen, Kratz-Cess and the Modified Lacis-Hansen Parameterizations for Two Solar Zenith Angles

	$\Theta_0 = 30°$		$\Theta_0 = 75°$	
	Direct	Total	Direct	Total
Line-by-line	168.4	178.1	68.2	71.4
Lacis-Hansen	154.3	162.3	62.5	63.6
Kratz-Cess	157.4	164.4	61.3	62.1
Modified Lacis-Hansen (this study)	170.1	178.7	68.5	69.7

Values are in watts per square meter. Surface albedo is 0.2.

TABLE 2. Coefficients and Weights for the 11 Pseudo-Monochromatic Intervals in the Exponential-Sum-Fit Representation of the Solar Water Vapor Transmission in the Atmosphere, According to the Modified Lacis-Hansen Scheme Developed in This Study

Interval	Coefficient m^2/kg	Weight
1	4.0000E−6*	
2	2.0000E−4	
3	3.5000E−3	
4	3.7700E−2	
5	1.9500E−1	
6	9.4000E−1	
7	4.4600E0	
8	1.9000E1	
9	9.8900E1	
10	2.7060E2	
11	3.9011E3	

Read 4.0000E−6 as 4.0000×10

Defining Tr_l^d and Re_l^d as the total transmissivity (i.e., accounting for direct and diffuse beams) and the reflectivity of the direct incident radiation by the cloud layer l, respectively, the downward flux at the cloud base (level $L + 1$) can be written as the sum of the direct

$$D_{L+1}^d = D_L^d \exp\left(-\frac{\tau_l}{\mu_0}\right) \tag{7}$$

and the diffuse (with appropriate superscripts)

$$D_{L+1}^f = D_L^d\left[\mathrm{Tr}_l^d - \exp\left(-\frac{\tau_l}{\mu_0}\right)\right] \tag{8}$$

components. Both Tr_l^d and Re_l^d depend on the cloud layer (Figure 2*b*) optical depth τ_l, which is the sum of the drop and the vapor optical depths (layer subscript for drop is suppressed),

$$\tau_l = \tau_{\mathrm{drop}} + \tau_{\mathrm{vap},l} \tag{9}$$

The downward flux at any level below the cloud base can be written separately for the direct (D^d) and the diffuse (D^f) beams emerging from the cloud layer. Thus at the surface (level N; Figure 2*b*), the direct component is

$$D_N^d = D_L^d\left(\exp\left(-\tau_l/\mu_0\right)\prod_{j=L+1}^{N-1} t_j^d\right) \tag{10}$$

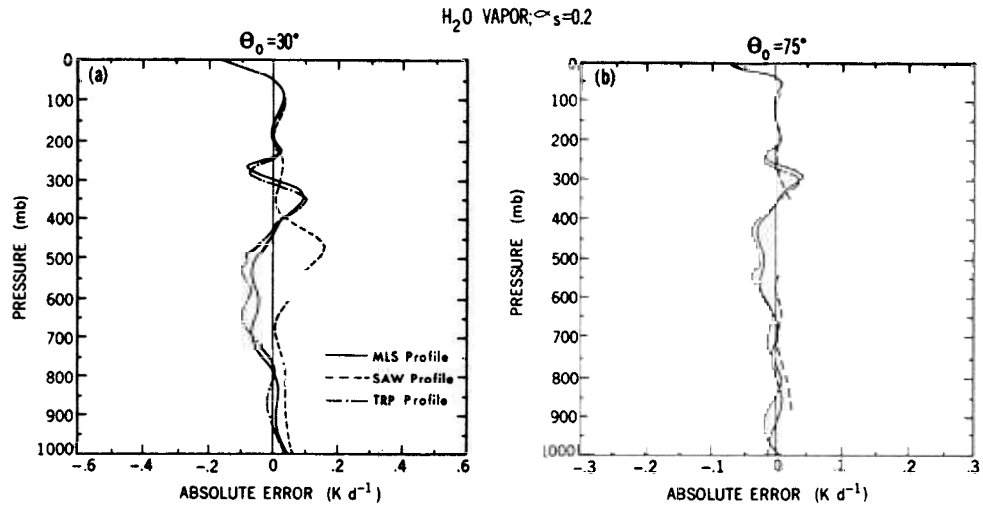

Fig. 5. Absolute errors in the vertical profile of the heating rate, as obtained with the modified Lacis-Hansen parameterization of the solar water vapor absorption for three different model atmospheres (MLS, mid-latitude summer; SAW, sub-Arctic winter; TRP, tropical). Solar zenith angles Θ_0 considered are (*a*) 30° and (*b*) 75°.

where the term t^d, defined by (2), refers to the transmission of the direct beam by the water vapor below the cloud. The diffuse component at the surface is

$$D_N^f = D_L^d \left[\prod_{j=L+1}^{N-1} t_j^f \right] \quad (11)$$

where the term t^f, defined by (5), refers to the transmission of the diffuse beam by the vapor below the cloud. The total flux at the surface is given by

$$D_N = (D_N^d + D_N^f) \quad (12)$$

The reflected flux at the cloud top is a diffuse beam and is given by

$$U_L = (D_L^d)(\mathrm{Re}_l^d) \quad (13)$$

while that at the top of the atmosphere, with the appropriate vapor transmission function t^f, is

$$U_1 = U_L \prod_{j=1}^{L-1} t_j^f \quad (14)$$

Expressions for intermediate level fluxes can be written down in a similar manner with appropriate changes in the indices of the water vapor transmission functions. The heating rates in the cloud layer l and in all the noncloud layers are as defined by (6). In these equations, the layer transmission (t, Tr) and the reflection (Re) functions are all that is needed to determine the solar flux disposition in the atmosphere. The bases for determining these functions are the spectrally dependent LBL vapor absorption coefficients and the drop single-scattering properties, namely, extinction optical depth τ_{drop}, single-scattering albedo ω, and phase function or asymmetry factor g.

The spectrally detailed inhomogeneous transfer over the relevant portion of the solar spectrum (0–18,000 cm^{-1}) can be performed according to the methods outlined by RF. The spectral resolution required to study vapor-drop interactions (~0.006 cm^{-1} [see RF]) is dictated by the fine absorption features of the water vapor molecule (Figure 1). In contrast, drop properties remain constant over broad spectral intervals (>100 cm^{-1}). The goal of preparing reference results for the testing and development of parameterizations also necessitates a large number of computations, involving a wide range in the values of the parameters related to clouds. Thus keeping in mind the computational requirements and the necessity to retain a high spectral resolution, we adopt here the line-by-line + delta-Eddington technique to prepare a set of reference results (for details on the method, the reader is referred to the VC2 technique described by RF). Although this method does not yield benchmark-quality results [RF], the solutions can represent a good approximation [*Fouquart et al.*, 1991]. Briefly, the technique performs the transfer at every discrete frequency point over which the water vapor lines are resolved, using the delta-Eddington approximation [*Joseph et al.*, 1976] to compute the multiple scattering properties for the cloud layer (i.e., reflection and transmission). The water vapor transmission in the other layers follows Beer's law at each frequency. Equations (7)–(14) are then employed to obtain the fluxes at each level and at each discrete frequency. This is followed by an integration over the spectrum [see RF].

The parameter space spanned here include clouds of different drop size distributions, optical depths, and thicknesses, located at different altitudes and illuminated at various solar zenith angles. The vapor profiles follow the *McClatchey et al.* [1972] mid-latitude summer specifications, except that layers containing clouds are assumed to contain vapor corresponding to saturation conditions. The cloud drop size distributions used in this study are the ICRCCM-specified CS and CL models [*Fouquart et al.*, 1991] and those stemming from *Slingo*'s [1989] study. The CS model is typical of a stratus cloud, while the CL model has higher concentrations of relatively large drops. The ICRCCM tables specify drop single-scattering properties at 97 distinct frequencies in the interval 0–18,000 cm^{-1} of the solar spectrum where water vapor, too, has absorption features. The solar irradiance data for the ICRCCM models follows *Labs and Neckel* [1970], with the total flux for normal incidence at the top of the atmosphere over the 0- to

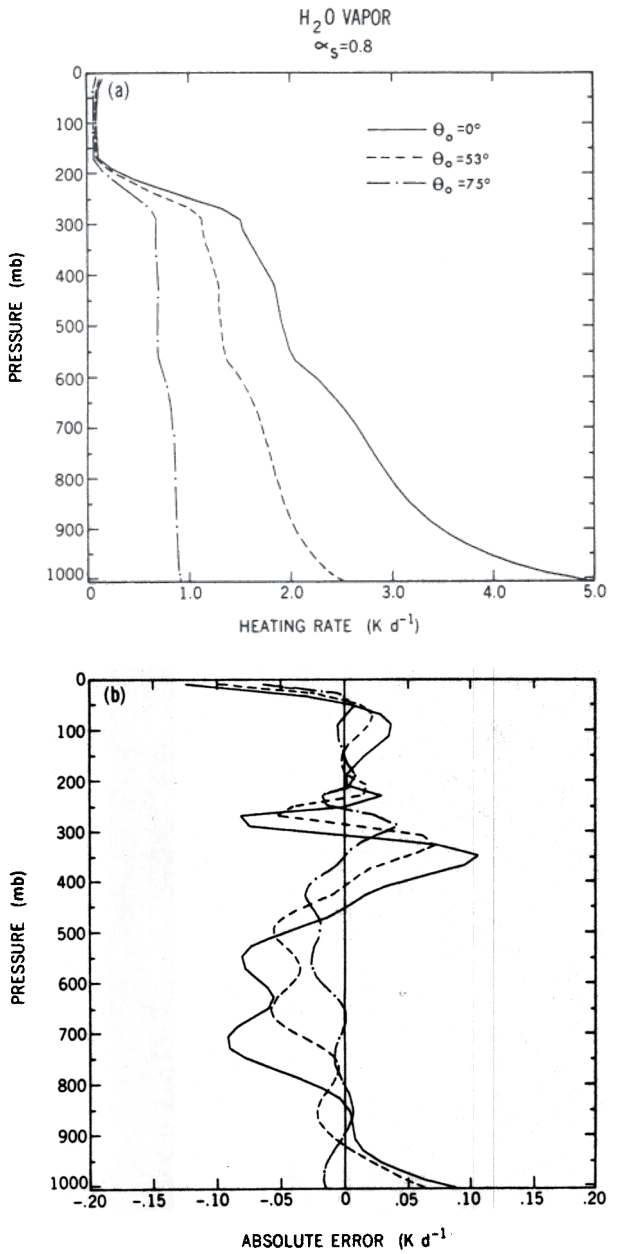

Fig. 6. (*a*) LBL values of the heating rate due to solar absorption by water vapor in a mid-latitude summer atmosphere for three different solar zenith angles (surface albedo $\alpha_s = 0.8$) (*b*) Absolute error at each zenith angle due to the modified Lacis-Hansen parameterization.

18,000-cm^{-1} spectrum being 966 W/m^2. (For completeness, we consider the spectrum to be 0–18,000 cm^{-1}; the interval 0–1000 cm^{-1} contains a small amount of incident solar flux and can be ignored in practical considerations).

In Slingo's formulation, the single-scattering properties (his Table 1) are specified as functions of effective drop radius and liquid water path (LWP). These properties, together with the solar irradiance (total, 960 W/m^2), are specified at spectral intervals different from ICRCCM. As a note, the CS model's effective radius is ~5 μm, which is approximately the lower limit of applicability of the Slingo scheme. The upper limit for the effective radius in Slingo's scheme is 15 μm.

The range in zenith angles considered in this study is 0° to 75°. The range in drop optical depths studied is 1 to 100, which implies a range of ~3.5–350 g/m^2 for the CS model. As in RF, the drop extinction optical depth refers to the value at 0.55 μm; optical depths at other wavelengths for the ICRCCM model reference computations are obtained by using the ratio of the extinction coefficient values at the different wavelengths to the value for the 0.55-μm wavelength. For the reference calculations corresponding to the Slingo drop model, a specific value of the optical depth at 0.55 μm is used to infer a LWP which, in turn, yields the single-scattering values at all other wavelengths.

4. Broadband Treatment of Overcast Sky Interactions

The simplicity of the broadband water vapor absorption formulation of LH has sparked the search for a similar formalism applicable to overcast skies so that the near-infrared radiative transfer can be handled with computational ease in climate and weather prediction models. Because the water vapor absorption parameterization is formulated on a broadband basis, the drop radiative properties, too, are constrained to have a broadband representation. This requires that drop reflection and transmission be an accurate measure of the integrated effects over the 0- to 18,000-cm^{-1} spectrum. In order to proceed with the broadband concept, several important considerations become necessary and need to be addressed, as described below.

4.1. *Multiple-Scattering Method*

An efficient yet sufficiently accurate method is required to obtain the multiple-scattering radiative properties at any discrete frequency or over a spectral interval. Our choice here is the delta-Eddington method [*Joseph et al.*, 1976]; its accuracy has been tested by *King and Harshvardhan* [1986] for drop-only situations. In this study, both the reference results (section 3) and the broadband parameterizations employ the delta-Eddington method.

4.2. *Drop Broadband Radiative Properties*

It is necessary to consider the wavelength dependence of the drop single-scattering properties and, from these, to obtain the drop broadband radiative properties. The parameter of prime importance in this regard for water clouds is the single-scattering albedo, since it alone has an extremely significant variation across the spectrum [*Chylek et al.*, 1984; *Slingo*, 1989; *Fouquart et al.*, 1991; RF]. The single-scattering quantities may be calculated by considering a drop size distribution and Mie theory, such as the ICRCCM or the Slingo tabulations.

One method to arrive at broadband drop properties is to compute the reflectivity and transmissivity at each spectral interval using relevant drop spectral single-scattering quantities and then perform the integration over the spectrum. This involves delta-Eddington calculations over more than one spectral interval. Referring to equations (7)–(14), the corresponding expressions for the transfer in the broadband sense are similar except that Tr and Re terms, which were obtained for the layer as a whole (i.e., drop + vapor), have to be replaced by the terms T and R, respectively, defined for drops only. T refers to the total (direct + diffuse) beam transmission by the drops. Further, a spectral average of

TABLE 3. Spectral Intervals Adopted in This Study for Computing the Broadband Drop Multiple-Scattering Properties of the CS and CL Drop Models

Spectral Interval, cm^{-1}	Solar Irradiance, W/m^2	Extinction Coefficient, km^{-1}	Single-Scattering Albedo	Asymmetry Factor
		CS Drop Model		
0–1961	6.024	1.95	0.922419	0.510
1961–3846	35.588	49.07	0.710540	0.846
3846–5556	72.079	46.25	0.977083	0.809
5556–6250	41.396	43.69	0.996321	0.782
6250–7143	59.149	43.35	0.995298	0.790
7143–8333	82.128	43.20	0.996701	0.795
8333–10,000	120.114	42.07	0.999670	0.803
10,000–10,204	14.944	41.58	0.999784	0.798
10,204–10,526	23.663	41.78	0.999744	0.794
10,526–10,753	16.686	41.64	0.999850	0.800
10,753–18,000	494.658	41.11	0.999986	0.824
		CL Drop Model		
0–1961	6.024	114.40	0.671521	0.700
1961–3846	35.588	127.46	0.595724	0.884
3846–5556	72.079	126.04	0.889218	0.837
5556–6250	41.396	124.55	0.980510	0.829
6250–7143	59.149	123.71	0.976421	0.834
7143–8333	82.128	123.17	0.984021	0.838
8333–10,000	120.114	121.31	0.998522	0.835
10,000–10,204	14.944	121.36	0.999225	0.828
10,204–10,526	23.663	121.67	0.999155	0.835
10,526–10,753	16.686	121.91	0.999470	0.843
10,753–18,000	494.658	121.76	0.999953	0.854

The solar irradiance, the extinction coefficient, the single-scattering albedo and the asymmetry factor associated with each interval are also listed.

these quantities is now necessary over the entire 0- to 18,000-cm^{-1} ($=\Delta\nu$) spectrum. The drop reflectivity and transmissivity of the incident direct beam are given by

$$\frac{\int_{\Delta\nu} R^d(\nu)F_0(\nu)\,d\nu}{\int_{\Delta\nu} F_0(\nu)\,d\nu} \tag{15}$$

$$\frac{\int_{\Delta\nu} T^d(\nu)F_0(\nu)\,d\nu}{\int_{\Delta\nu} F_0(\nu)\,d\nu} \tag{16}$$

where $F_0(\nu)$ is the extraterrestrial solar radiation at frequency ν, the overbars denote spectrally averaged quantities, and the subscript 0 for $\bar{R}$ and $\bar{T}$ indicates that the spectral averages are obtained with the top-of-the-atmosphere incident solar flux as the weighting function. As before, the superscript d defines the properties with respect to direct incident radiation. R^d and T^d are dependent only on the frequency ν via the single-scattering parameters. In (15) and (16), $\bar{R}_0$ and $\bar{T}_0$ are functions of only the drop single-scattering parameters and the solar zenith angle. The ICRCCM specifications for the CS and CL drop models lists values over 97 different intervals in the near-infrared spectrum (0–18,000 cm^{-1}). We have reduced the number of intervals to 11 in this study. The rearrangement of the intervals is accompanied by an arithmetic average of the single-scattering properties (see Table 3). One exception to this procedure is the first interval in Table 3 where the single-scattering values are chosen so as to match the band multiple-scattering quantities obtained using the original set. Computations of the 0- to 18,000-cm^{-1} cloud reflectivity, transmissivity, and absorptivity are in error by only a few percent (4% in absorption and <1% in reflection and transmission) for drop optical depths ranging from 1 to 100 and for sun angles from 0° to 75°, when compared with the full 97-interval results. *Slingo* [1989] also demonstrates the use of a few spectral intervals for the accurate simulations of drop multiple scattering properties.

Another way to obtain near-infrared drop properties is to define broadband values of the single-scattering parameters themselves. The latter can be combined with the vapor optical depth, and then a two-stream approximation can be employed to obtain the cloud layer reflection and transmission [LH; *Harshvardhan et al.*, 1987]. This concept is investigated in section 6.

4.3. *Spectral Attenuation Above Cloud*

It is necessary to consider the influence of the solar spectral attenuation by the water vapor above the cloud on the drop broadband effects. The employment of a broadband water vapor absorption scheme implies that there is a complete loss of information about the spectral distribution of the near-infrared irradiance in the atmosphere, i.e., at any level, it is not possible to associate a definite amount of solar flux with a particular frequency interval. The loss of the spectral information acquires importance because each frequency band undergoes a distinctly different attenuation [RF]. This significance becomes more crucial when overcast skies are considered. As was pointed out by *Fouquart et al.*

[1991], the sharp spectral variation of the drop single-scattering coalbedo introduces an additional spectral dependence in the radiative transfer for the inhomogeneous atmosphere (see Figure 1), besides that arising due to solar irradiance and vapor absorption. While it can be argued from the results of section 2 that the latter two are well accounted for in the broadband framework for a cloudless atmosphere and that the broadband convolution of the solar irradiance with drop properties also can be treated with ease (section 4.2), the same is not necessarily true when vapor and droplets are present simultaneously. This is because the correlation in the strengths of the vapor and drop absorption can be quite different in the various near-infrared spectral intervals [RF].

To examine the quantitative nature of such effects, consider the broadband transfer in the inhomogeneous atmosphere with a cloud located in the lth layer and no vapor inside the cloud. The drop reflectivity and transmissivity with respect to the incident direct beam (identified again by superscript d) are then given by

$$\bar{R}_l^d = \frac{\int_{\Delta\nu} R^d(\nu) D_L^d(\nu)\, d\nu}{\int_{\Delta\nu} D_L^d(\nu)\, d\nu} \tag{17}$$

$$\bar{T}_l^d = \frac{\int_{\Delta\nu} T^d(\nu) D_L^d(\nu)\, d\nu}{\int_{\Delta\nu} D_L^d(\nu)\, d\nu} \tag{18}$$

Equations (17) and (18) are defined similar to (15) and (16), respectively, except that the weighting function is now the frequency-dependent incident flux at the cloud top, $D_L^d(\nu)$, not that at the top of the atmosphere, $F_0(\nu)$. If the position of the cloud in the atmosphere is specified, one could in principle obtain $D_L^d(\nu)$ from the reference results and then solve for (17) and (18). However, $D_L^d(\nu)$ is not available on a general basis, and so there exists a problem in the determination of $\bar{R}_l$ and $\bar{T}_l$ for arbitrary cloud locations in the atmosphere. Usual calculations of drop radiative properties [e.g., *Slingo*, 1989] yield only $\bar{R}_0$ and $\bar{T}_0$, that is, the radiative properties as if there were no water vapor above the cloud, and with only drops being present in the atmosphere. The parameters, $\bar{R}_l$ and $\bar{T}_l$ can differ considerably from $\bar{R}_0$ and $\bar{T}_0$, respectively, and from the ratio

$$\left(\frac{\bar{R}_l}{\bar{R}_0}\right)^d = \frac{\int_{\Delta\nu} R^d(\nu) D_L^d(\nu)\, d\nu}{\int_{\Delta\nu} R^d(\nu) F_0(\nu)\, d\nu} \frac{\int_{\Delta\nu} F_0(\nu)\, d\nu}{\int_{\Delta\nu} D_L^d(\nu)\, d\nu} \tag{19}$$

and the analogous one for $(\bar{T}_l/\bar{T}_0)^d$

$$\left(\frac{\bar{T}_l}{\bar{T}_0}\right)^d = \frac{\int_{\Delta\nu} T^d(\nu) D_L^d(\nu)\, d\nu}{\int_{\Delta\nu} T^d(\nu) F_0(\nu)\, d\nu} \frac{\int_{\Delta\nu} F_0(\nu)\, d\nu}{\int_{\Delta\nu} D_L^d(\nu)\, d\nu} \tag{20}$$

it is apparent that if R^d and T^d are independent of frequency, (19) and (20) reduce to unity with no dependence on altitude. The same result would be obtained if the vapor absorption were independent of frequency (i.e., gray absorber). Then, $D_L^d(\nu)$ is related to $F_0(\nu)$ through a constant. However, neither aspect is true in general because there does occur a strong frequency dependence for R^d, T^d, and the vapor absorption. Not only is $D_L^d(\nu)$ frequency-dependent, but it also decreases with increasing pressure, causing both the numerator and the denominator in (19) and (20) to be dependent on the amount of vapor above the cloud encountered by the direct solar beam.

The variation of the ratios (19) and (20) with the CS model drop optical depth and vertical location is illustrated in the left-hand panels of Figures 7 and 8, respectively, for solar zenith angles of 0° and 75°. These computations are performed in the same manner as described in section 3, except that in-cloud vapor is assumed absent in order to isolate the role of the above-cloud vapor. For thick optical depths (>10), the $D_L^d(\nu)$ integral in the denominator of (19) falls off more rapidly with increasing pressure than does the integral in the numerator. For thin optical depths, the variations in the numerator, too, can be significant, thus slowing the increase of the ratio (19) with pressure, and even causing a decrease. In the case of the ratio (20), the same features are noticed except that the $\bar{T}/\bar{T}_0$ values exhibit a monotonic increase with pressure for all optical depths. With the ratios (19) and (20) being >1, the broadband drop reflectivity and transmissivity for a location "l" inside the atmosphere are greater than the values in the absence of the above-cloud vapor. Consequently, ignoring the influences due to the above-cloud vapor on the broadband drop properties would result in an overestimate of the cloud absorptivity.

The resulting effects on the cloud layer heating rates are investigated with respect to the reference values (Figures 7 and 8) for 20-mbar-thick clouds at different heights. The relative errors (Figure 9) illustrate the unacceptably large differences at both sun angles due to the use of $\bar{R}_0$ and $\bar{T}_0$ instead of $\bar{R}_l$ and $\bar{T}_l$. The relative errors decrease with drop optical depth and consist of an overestimate in the heating within the clouds. The overestimates are greater for low clouds and for high zenith angles, i.e., when the above-cloud vapor paths are large. The salient point of Figure 8 is that the spectral attenuation by the above-cloud vapor affects the determination of the broadband drop reflection and transmission. Failure to account for this effect properly causes a misrepresentation of the radiative properties, with unrealistically more radiation being absorbed by the drops.

Note that the errors occur despite the fact that the flux absorbed by the vapor above the cloud in the modified LH scheme is well simulated. If we use the original LH vapor absorption formulation, which underestimates the broadband above-cloud vapor absorption (section 2), more flux is incident at cloud top and the cloud heating overestimates in the lower troposphere become even more severe (e.g., for a cloud at 900–920 mbar of optical depth 10, the error is 150% at normal solar incidence).

To account for this influence of the water vapor above the cloud, $\bar{R}_l/\bar{R}_0$ and $\bar{T}_l/\bar{T}_0$ have been parameterized using the reference values obtained for a solar zenith angle of 53°. On the basis of off-line tests, it is assumed that these ratios hold true for all solar zenith angles,

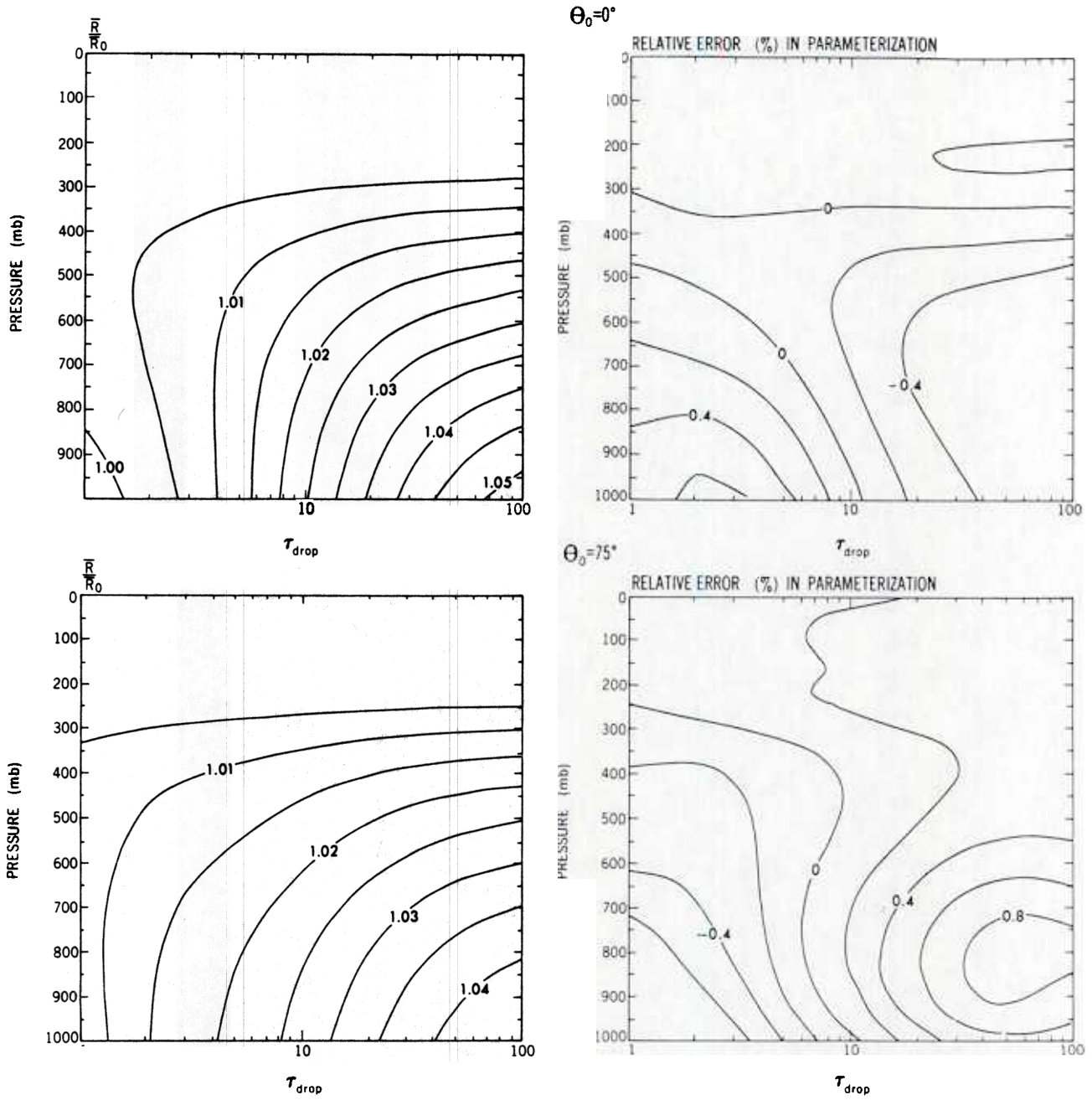

Fig. 7. Reference value of the ratio $\bar{R}/\bar{R}_0$ and the relative error (%) in the parametric fits (Table 4)), for overcast atmospheres illuminated by (top) the overhead sun ($\Theta_0 = 0°$), and (bottom) $\Theta_0 = 75°$, as a function of drop optical depth (τ_{drop}) and cloud location in the atmosphere (see section 4.3).

$$\bar{R}_l^d(W_v, \mu_0, \tau_{drop}) = \left(\frac{\bar{R}_l}{\bar{R}_0}\right)_{53}^d \bar{R}_0^d \tag{21}$$

$$\bar{T}_l^d(W_v, \mu_0, \tau_{drop}) = \left(\frac{\bar{T}_l}{\bar{T}_0}\right)_{53}^d \bar{T}_0^d \tag{22}$$

where $\bar{R}_l/\bar{R}_0$ (equation (19)) and $\bar{T}_l/\bar{T}_0$ (equation (20)) are explicit functions of the drop optical depth (derived here for the ICRCCM CS and CL models), and the slant water vapor path above the cloud top,

$$W_v = \frac{1}{\mu_0 g_0} \int_0^{P_L} q_l \, dp_l \tag{23}$$

The parametric relationships for (21) and (22) are listed in Table 4 for the CS and CL drop models. The right-hand panels of Figure 7 and 8 illustrate the relative errors in the parametric fits as a function of cloud location and optical depth. They also depict the impact of using the 53° results to represent the ratios at other angles. At 53° itself (not shown), for the parameter space considered, the errors for $\bar{R}_l/\bar{R}_0$ and $\bar{T}_l/\bar{T}_0$ range from −0.2 to 0.2% and −0.4 to 0.6%, respec-

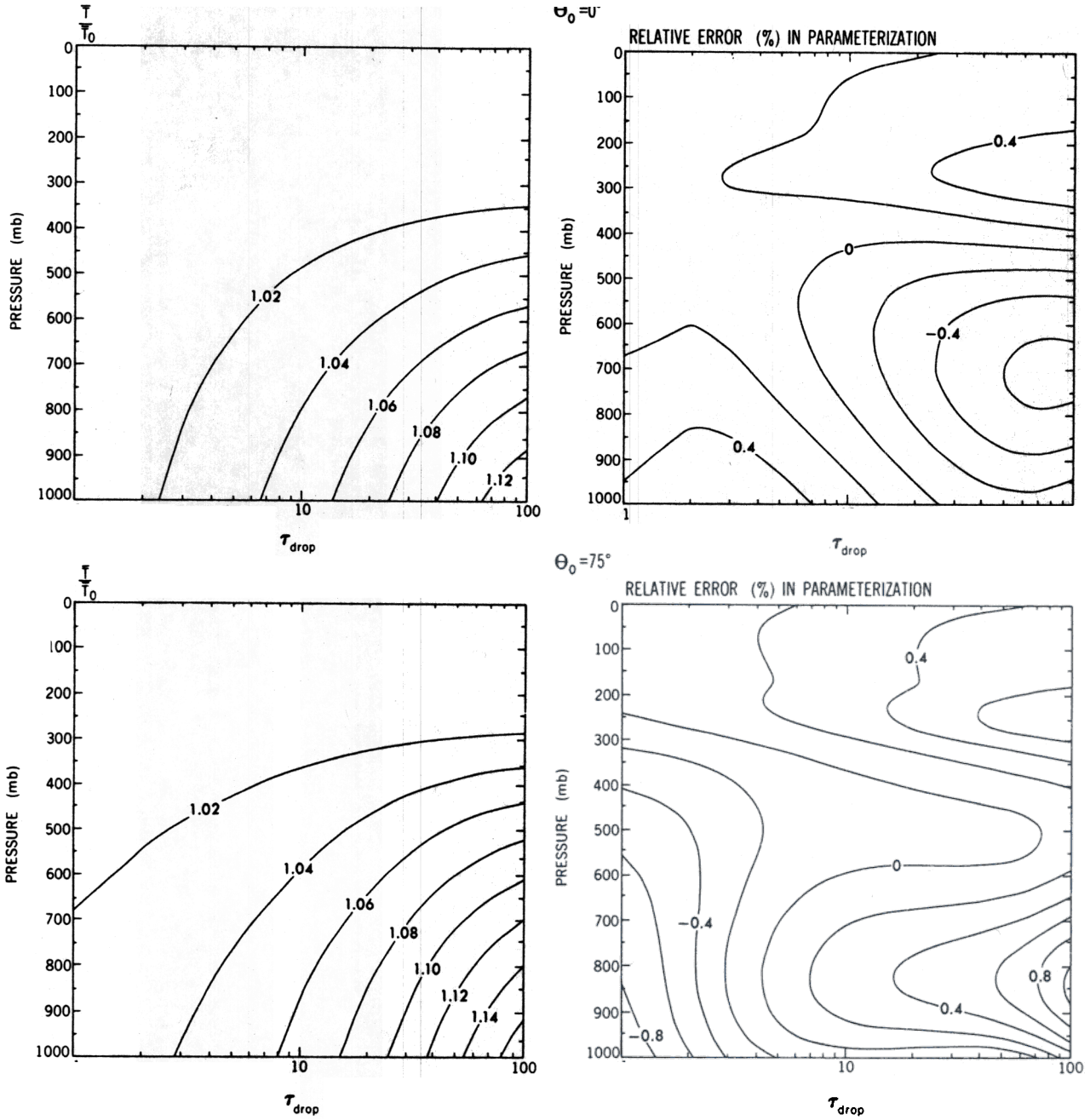

Fig. 8. Same as for Figure 7, except for $\bar{T}/\bar{T}_0$.

tively. For low zenith angles and small optical depths, the reflection and transmission are overestimated, while at large optical depths, both are underestimated. For large zenith angles, the converse of the effect at 0° prevails. The behavior is similar for the CL cloud and is not illustrated. Note that ignoring the above-cloud vapor effects is equivalent to equating (21) and (22) with (15) and (16), respectively.

The preceding discussions pertain only to the direct solar flux incident on the cloud. In the case of multiple reflections such as due to a surface or a cloud present elsewhere in the atmosphere, equations (17)–(20) have to be redefined. In this case, it is necessary to consider not only the spectral depletion of the beam above cloud but also that due to multiple reflections between clouds and/or surface. This is a complicated issue that is not easily resolved in the broad-band framework. However, a prescription for handling such problems is given in section 7.

4.4. *Rescaling of Parameters*

Depending on the multiple-scattering approximation employed, a rescaling of the single-scattering parameters and the direct flux may become necessary. For example, under the delta-Eddington approximation, the parameter τ_{drop} has to be replaced by the scaled optical depth τ^*_{drop} in each of the intervals of Table 3, based on the definition of *Joseph et al.* [1976]

$$\tau^*_{drop} = (1 - g^2\omega)\tau_{drop} \qquad (24)$$

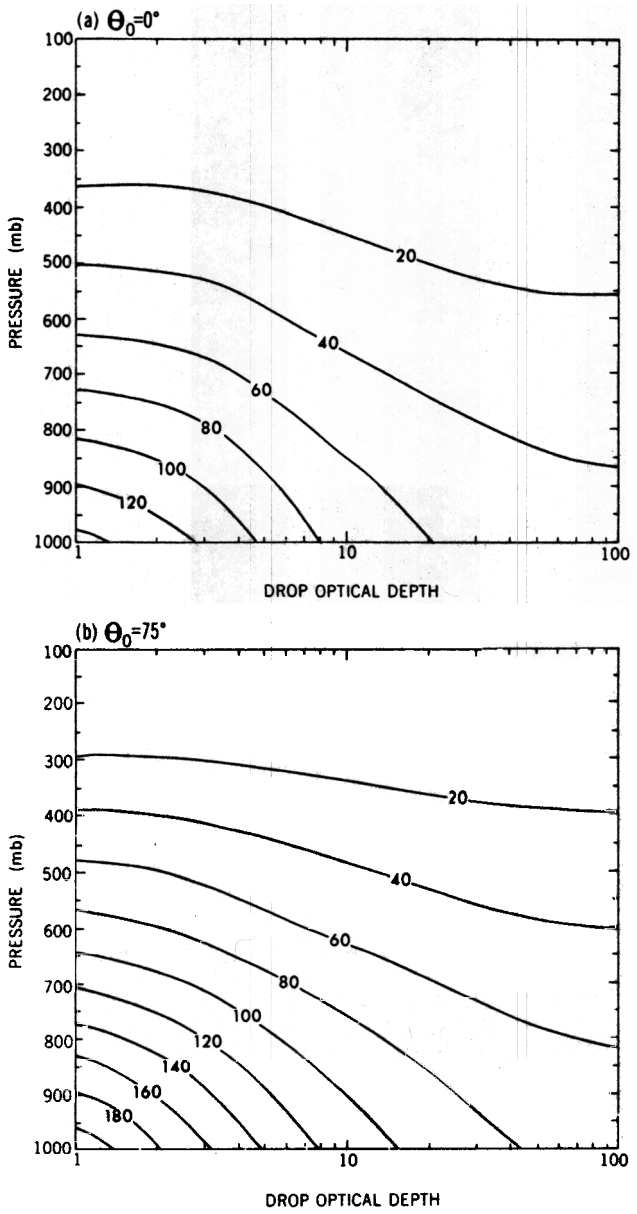

Fig. 9. Relative errors (percent) in the heating rate within a 20-mbar-thick CS cloud of various drop optical depths and located at different altitudes, when the influence of the above-cloud vapor in formulating the reflectivity and transmissivity characteristics of the drops is ignored (see section 4.3). Solar zenith angles Θ_0 considered are (*a*) 0° and (*b*) 75°. In-cloud water vapor is ignored in these calculations.

where the relation for the Henyey-Greenstein phase function has been assumed. The scaled "direct" transmission in each interval is given by

$$\exp(-\tau^*_{\text{drop}}/\mu_0) = \exp\{-[\tau_{\text{drop}}(1-\omega g^2)]/\mu_0\} \quad (25)$$

Equation (25) has a sharp spectral dependence due to ω. If there were no water vapor above the cloud, then it would be trivial to obtain the appropriate broadband value

$$\overline{\exp(-\tau^*_{\text{drop}}/\mu_0)} = \frac{\int_{\Delta\nu} \exp(-\tau^*_{\text{drop}}(\nu)/\mu_0) F_0(\nu)\, d\nu}{\int_{\Delta\nu} F_0(\nu)\, d\nu} \quad (26)$$

However, in the presence of vapor above cloud, the irradiance at the cloud top varies with cloud altitude so that F_0 appearing in (26) has to be replaced by $D^d_L(\nu)$. This leads to a situation analogous to that for (17) and (18). In this study we ignore this variation and adopt the spectrally integrated mean value of the exponential quantity as defined by (26). The actual numerical integration in (26) is performed using the data in Table 3. The errors due to this approximation are unlikely to be important when drop optical depths $\gg$1 are involved.

4.5. *Water Vapor Inside Cloud*

It is necessary to consider the role of the water vapor inside the cloud and the accompanying vapor-drop interactions. The importance of this effect is assessed by comparing reference heating rate calculations with and without vapor in the cloud layer. The difference between these results is a measure of the influence of water vapor inside the cloud layer. Figure 10 illustrates the percentage increase in the absorption due to the in-cloud vapor for 20-mbar-thick CS cloud layers of different optical depths and located at various altitudes. Clearly, for clouds of drop optical depth <10, and particularly in the lower troposphere where the saturation vapor mixing ratios are larger, the presence of in-cloud vapor contributes significantly to the total cloud absorption.

The incorporation of the spectrally dependent effects due to the drops and the in-cloud vapor into a joint broadband framework is a challenging task. Besides having a distinctly different spectral dependence (Figure 1), they also differ in their radiative properties: one is a pure absorber while the other absorbs and scatters radiation. Several models (especially GCMs) that have employed the broadband LH water vapor parameterization have been forced to make several assumptions that are sometimes not explicitly stated.

One of these assumptions is that the cloud reflection is independent of the vapor inside the cloud. The rationale for this assumption appears to be based on the following premise: the water vapor optical depths are sufficiently small so that the reflection is dominated entirely by the drop single-scattering properties. Further, the spectral bands contributing to reflection are assumed to be displaced from those causing absorption inside the cloud.

The second approximation invoked for the broadband parameterization concerns the transmission through the cloud layer. The total transmission of the cloud layer is assumed to be given by the product of two separate transmission functions: the transmissivity of the drops and that due to vapor. This is analogous to the overlap treatment for gases [*Goody and Yung*, 1989]. Conceptually, the two assumptions amount to incident radiation traversing two hypothetical sublayers within the cloud, the first one containing drops only, the second containing only vapor.

The validity of these approximations is investigated by performing computations similar to the reference calculations (section 3), except it is now assumed that the cloud layer reflection is dependent only on the drop characteristics while the cloud (drop + vapor) transmission follows the multiplicative formulation stated above. This "approximate" reference result is then compared with the corresponding complete reference result. The relative errors due to the assumptions concerning the role of the in-cloud vapor are listed in Table 5 for drop optical depths of 1, 10, and 100

TABLE 4. Coefficients in the Parameterization of the Expressions $\bar{R}/\bar{R}_0$ and $\bar{T}/\bar{T}_0$ (Equations (19) and (20)) Used to Obtain the Drop Radiative Properties (Equations (21) and (22) at Any Location in the Atmosphere

Coefficient	A	B	C	D	E	F
			CS Drop Model			
a	0.0164	−0.0138	−0.182	−0.0427	0.0103	−2.719
b	0.3370	−0.1480	−0.395	−0.0420	0.7620	−1.889
c	0.0041	0.0152	−2.022	0.0405	6.2800	−5.093
p	0.0435	−0.0395	−0.107	−0.0206	0.0110	−4.315
q	0.3250	0.0069	0.510	−0.0010	0.0213	−3.314
r	0.0010	0.0017	0.152	−0.0036	−0.0013	−1.255
			CL Drop Model			
a	0.0249	−0.0165	−0.224	−0.0464	0.0121	−3.899
b	0.3590	−0.0818	−0.320	−0.0373	0.1050	−4.428
c	0.0041	0.0006	−1.411	0.0402	−0.048	−14.36
p	0.0431	−0.0378	−0.170	−0.0361	0.0193	−4.202
q	0.4010	−0.0906	−0.158	−0.0242	0.0831	−4.665
r	0.0002	0.0025	0.167	−0.0068	−0.0003	−0.237

The parameterized equations, with $\eta = \tau_{drop}$, and valid for $1 < \eta < 100$ and $0 < W_v < 116$ kg/m^2, are of the form $(\bar{R}/\bar{R}_0) = 1 + aW_v^b \exp(-cW_v)$ and $(\bar{T}/\bar{T}_0) = 1 + pW_v^q \exp(-rW_v)$, where W_v is the slant water vapor path (equation (23)) from the top of the atmosphere down to cloud top for a particular solar zenith angle and a, b, c, p, q and r are represented by $A + B\eta^C \exp(D\eta) + E \exp(F\eta)$. The values of A, B, C, D, E, and F for each of the coefficients a, b, c, p, q, and r are listed for the CS and CL drop models.

and for zenith angles of 0° and 75°, with the cloud located between 900 and 920 mbar. The agreement between the two methods is excellent for both the flux at the surface and that at the top of the atmosphere (errors <3%). The reflected flux, in particular, is affected only marginally by the presence of vapor in the cloud; this feature holds substantially even for somewhat larger vapor amounts (not shown). This result offers a valuable suggestion for the simple representation of reflection by clouds containing vapor and drops. The transmitted flux at the surface is also affected negligibly by the assumptions. The absorbed flux is underestimated up to 18%, and this reiterates the importance of the in-cloud vapor for the cloud layer absorption, especially at the smaller drop optical depths. It is clear from both Figure 10 and Table 5 that the effects of the in-cloud vapor must be accounted for in a proper manner.

The nature of the errors arising in the case of the spectrally detailed transfer discussed above suggests the potential application of the approximation to the broadband computations as well. When the assumptions are applied together with the modified LH water vapor absorption scheme (section 2), the droplet broadband direct transmission (26) is multiplied by the direct transmission due to water vapor (equation (2)) in the layer l to obtain the net direct transmission by the cloud (i.e., drops + vapor)

$$\bar{T}_l^d(\text{net}) = \exp(-\tau_{\text{vap},l}/\mu_0)\ \overline{\exp(-\tau^*_{\text{drop}}/\mu_0)} \quad (27)$$

This procedure is performed for each of the 11 intervals in Table 2. Likewise, for each interval, the droplet broadband diffuse transmission, obtained from (22) and (26), is multiplied by the diffuse transmission due to water vapor to obtain the net diffuse transmission by the cloud,

$$\bar{T}_l^f(\text{net}) = [\bar{T}_l^d - \overline{\exp(-\tau^*_{\text{drop}}/\mu_0)}]\ t_l^f \quad (28)$$

where t_l^f (equation (5)) represents the transmission of the diffuse beam (i.e., scattered at least once and assumed to be isotropic) by the vapor in the cloud layer l. It may be noted that this expression for treating the drop + vapor effects is somewhat different conceptually from the scheme outlined for cloudy atmospheres by LH [see *Harshvardhan et al.*, 1987]; the latter method is examined in section 6. The preceding discussions also imply that in the broadband framework, the reflectivity of the cloud layer in each interval of Table 2 is the same (namely, $\bar{R}_l^d$; equation (21)), in contrast to the transmissivity (equations (27) and (28)).

5. Application and Accuracy of the Present Parameterization

Based on the analyses in section 4, a recipe for the broadband radiative transfer treatment in the case of single cloud decks above a nonreflecting surface can be prescribed as follows, given the ICRCCM drop single-scattering properties, cloud location, thickness, and sun angle:

1. Obtain $\bar{R}_0^d$ (equation (15)) and $\bar{T}_0^d$ (equation (16)) using Table 3 and the delta-Eddington approximation.
2. Use the parametric representations (Table 4) to obtain the corrected drop broadband properties, $\bar{R}_l^d$ and $\bar{T}_l^d$ (equations (21) and (22)), based on the water vapor amount above the cloud (equation (23)), the solar zenith angle, and the drop optical depth.
3. Obtain the broadband direct beam transmission by the drops (equation (26)).
4. Obtain the net direct and diffuse transmission by the cloud layer, $\bar{T}_l^d$ (net) and $\bar{T}_l^f$ (net), respectively (equations (27) and (28)), for each of the 11 pseudo-monochromatic intervals in Table 2; these depend on the in-cloud vapor amount. Note that the diffuse beam is assumed to be isotropic.
5. Obtain the direct (equation (2)) and the diffuse (equation (5)) beam transmissions due to vapor in the noncloud layers, using the modified LH water vapor absorption scheme (section 2) and the pseudo-monochromatic intervals (Table 2).
6. Using equations (7)–(14), with $\bar{T}_l^d$(net) replacing exp

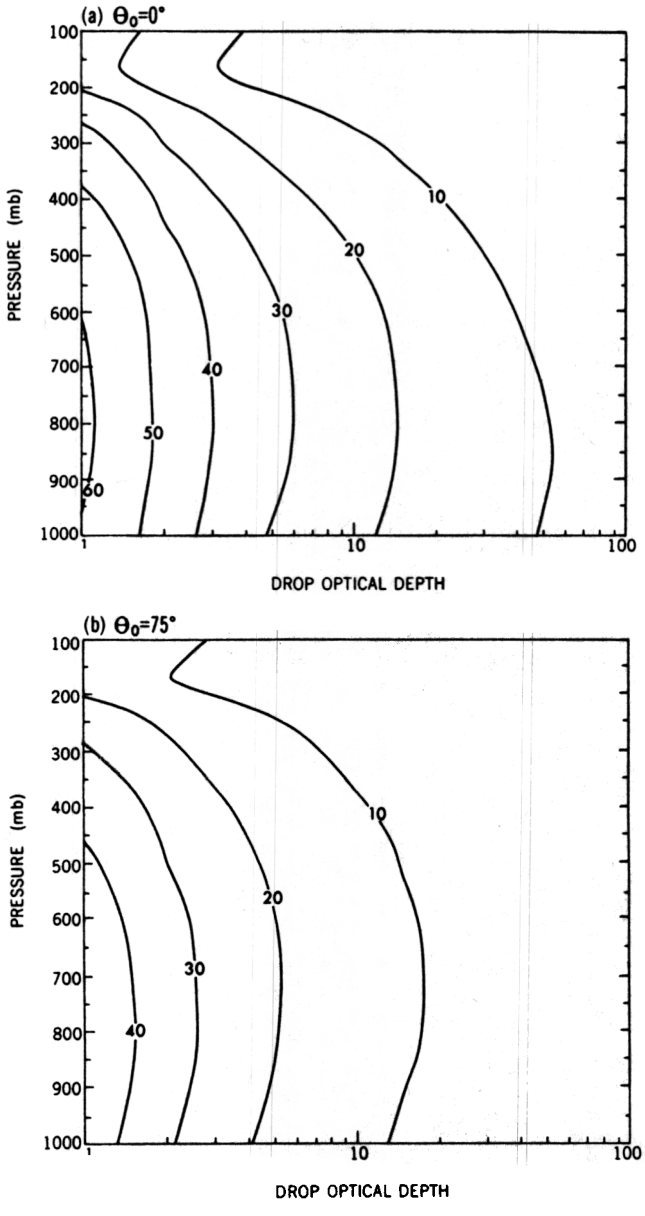

Fig. 10. Relative influence (percent) of the in-cloud water vapor on the absorption of solar radiation by 20-mbar-thick CS clouds, as a function of drop optical depth and vertical location (see section 4.5). Solar zenith angles Θ_0 considered are (*a*) 0° and (*b*) 75°.

$(-\tau_l/\mu_0)$, $\bar{T}_l^f$(net) replacing $(\mathrm{Tr}_l^d - \exp(-\tau_l/\mu_0))$, and $\bar{R}_l^d$ replacing Re_l^d, obtain the up and down fluxes for each pseudo-monochromatic interval, keeping track of the direct and diffuse beams separately.

7. Using the weights associated with each pseudo-monochromatic interval (Table 2), obtain the up and down solar fluxes in the atmosphere. Heating rates follow from application of (6).

5.1. *Tests With 20-mbar CS Clouds*

The accuracy of the recipe given above is investigated using the ICRCCM drop models in the mid-latitude summer atmosphere and for a range of conditions involving cloud locations and thicknesses and sun angles. First, tests are presented for 20-mbar-thick CS clouds with drop optical depths ranging from 1 to 100, and locations ranging from 100 to 1000 mbar. The study of 20-mbar cloud cases is consistent with the bases used for the parameterization of the above-cloud vapor effects in section 4.3. Zenith angles of 0°, 53°, and 75° are considered. All comparisons are with respect to reference results computed as described in section 3.

TABLE 5. Comparison of LBL+DE Computations (Incorporating the Assumptions Concerning Water Vapor Inside the Cloud Layer) With the Complete Reference LBL+DE Results (see Section 4.5)

	Relative Error, %					
	$\Theta_0 = 0°$			$\Theta_0 = 75°$		
	Q	F_{sfc}	F_{TOA}	Q	F_{sfc}	F_{TOA}
$\tau_{drop} = 1$	−1.7			−18.0		
$\tau_{drop} = 10$	−12.2			−8.4		
$\tau_{drop} = 100$	−6.8			−3.6		

The relative errors in the flux absorbed by the cloud layer (Q), the flux at the surface (F_{sfc}), and the reflected flux at the top of the atmosphere (F_{TOA}) are listed for CS drop optical depths (τ_{drop}) of 1, 10, and 100, located at 900–920 mbar. Solar zenith angles Θ_0 of 0° and 75° are considered.

The reference results and the relative error in the cloud layer heating rates (or, equivalently, the absorbed flux) due to the parameterization are shown in Figures 11, 12, and 13 for zenith angles of 0°, 53°, and 75°, respectively. Relative errors range from −20 to 30%, with the largest values occurring for low clouds with thin drop optical depths, particularly at the high zenith angle. On comparing Figure 9 with Figures 11 and 13 for $\tau > 3$, there is a substantial improvement when the cloud layer properties take into account the attenuation by the above-cloud vapor (the effect of the in-cloud vapor for these particular 20-mbar cases is less than that due to the above-cloud vapor).

The errors in the parameterized heating rates arise mainly due to (1) errors in the parametric fits (right-hand panels of Figures 7 and 8) which are more prominent for solar zenith angles other than 53° (section 4.3) and (2) errors in the approximations concerning the in-cloud water vapor, which affect the cloud layer absorption (section 4.5). The nature of effect 2, as pointed out earlier, leads to an underestimate in heating for low-lying clouds. From Figures 7 and 8, both R and T are overestimated at normal incidence for low clouds with drop optical depths <10 so that effect 1 also leads to an underestimate in the heating at the low zenith angle (Figure 11), while at the high zenith angle (Figure 13) there is a tendency to offset partially or even overcompensate for effect 2. For large drop optical depths (=100), the converse trends arise for effect 1 in Figures 7 and 8 and the significance of effect 2 is reduced as well (Figure 10). This results in a good simulation for the low clouds at normal incidence (Figure 11) and a slight underestimate for the 75° incidence (Figure 13).

Since parameterizations (21) and (22) are based on a solar zenith angle of 53°, Figure 12 indicates straightforwardly the improvement obtained as a result of accounting for the above-cloud vapor absorption through the use of the parametric fits (errors <10%). Further, since the higher altitude cloud cases shown in Figures 11–13 (say, above 500 mbar) are negligibly affected by the vapor above the cloud, the

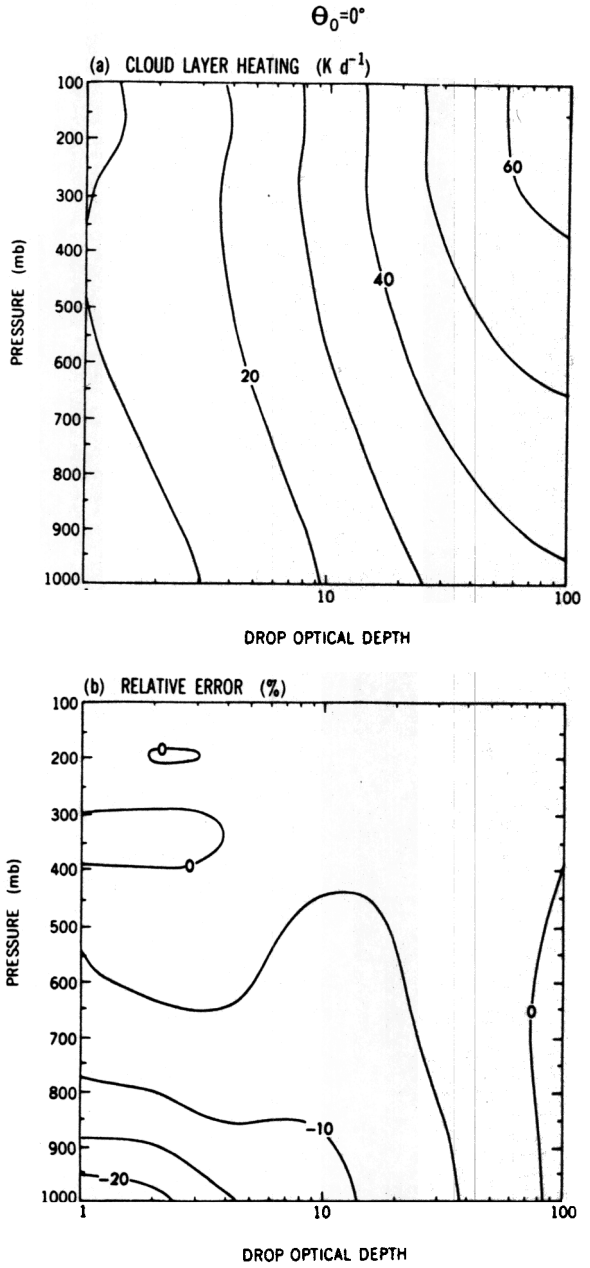

Fig. 11. (*a*) Reference values of the heating rate within a 20-mbar-thick CS cloud of various drop optical depths and located at different altitudes, as obtained from the reference results for overhead sun (Θ_0 = 0°). (*b*) Relative errors due to the parameterization developed in this study for overcast atmospheres (see section 5.1).

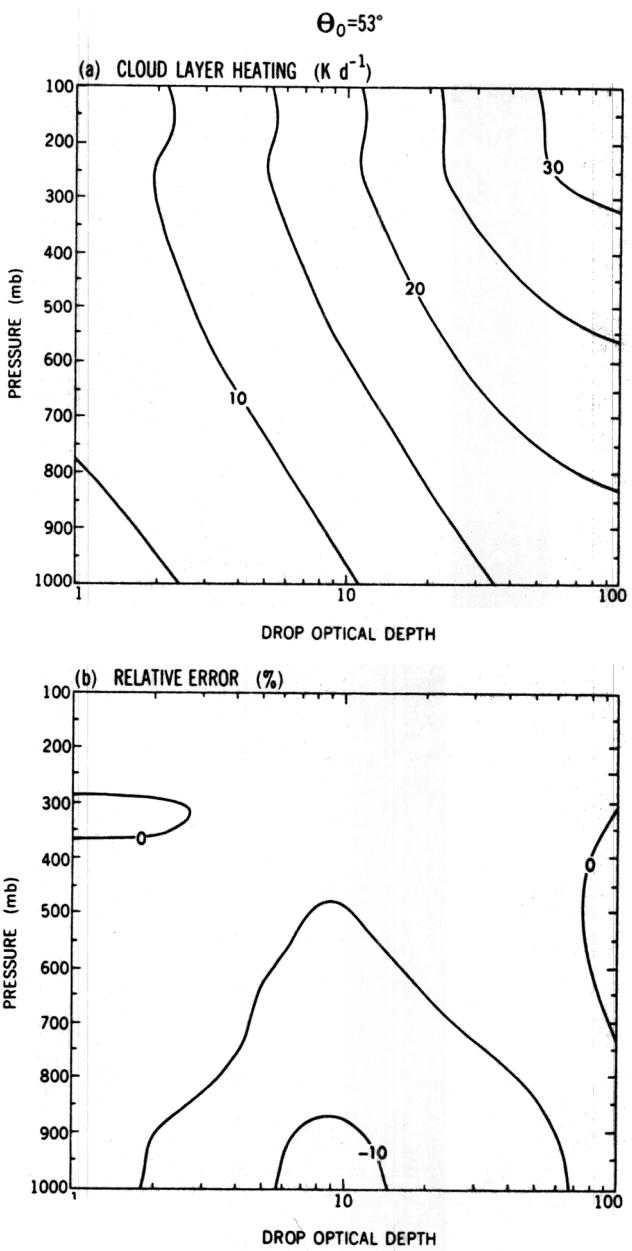

Fig. 12. Same as Figure 11, except Θ_0 = 53°.

results for such cases validate the concept of obtaining broadband values of $\bar{R}_0$ and $\bar{T}_0$ using merely 11 spectral intervals instead of the full 97 specified by ICRCCM. Both the above-cloud and the in-cloud vapor effects become more important for low-lying 20-mbar clouds due to increasing vapor paths (Figure 9) and vapor contents (Figure 10), respectively. Thus there is an increase in the errors with decreasing cloud height for all zenith angles.

The absolute errors, listed in Table 6, indicate that although the higher incident angles yield larger relative errors at the small optical depths, the discrepancies in the heating rate assume similar or more significance at normal incidence when there is a larger incident flux. This is true for any optical depth and altitude. The absolute errors are greater in magnitude for $\tau \sim 10$ (<2.5 K/d) (from Figures 11–13, the relative errors are <15% in this range). Table 6 suggests that the overhead sun, low cloud case with optical depth ~10 can be assumed to yield a fair representation of the maximum absolute errors for 20-mbar thick CS clouds in the present broadband parameterization.

We now turn our attention to the fluxes elsewhere in the model atmosphere. The vertical profile of the heating rate and the corresponding absolute errors are shown for 2 zenith angles, and a high and a low cloud case (τ_{drop} = 10) in Figure 14. The profiles for all other optical depths resemble that shown in Figure 14, with all of them being characterized by a pronounced peak at the cloud location. This reiterates the importance of the cloud absorption to the solar heating in overcast atmospheres. The absolute errors, too, have a peak in the cloud layer. This error is <2.5 K/d over the optical

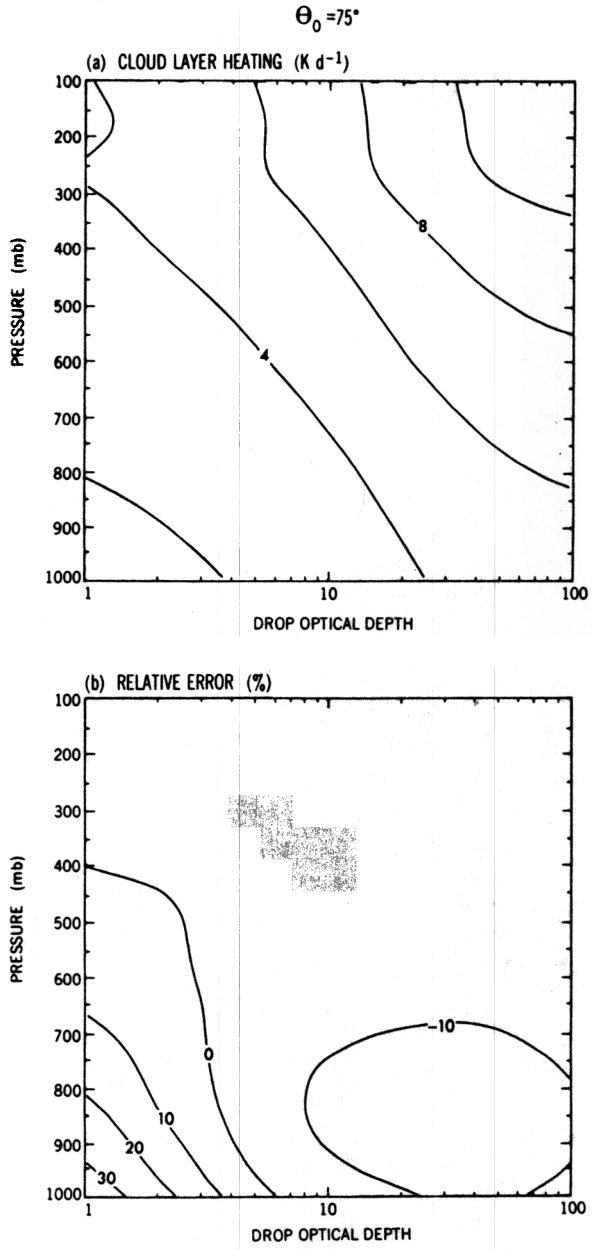

Fig. 13. Same as Figure 11, except Θ_0 = 75°.

depth range considered (1–100). The small errors in the noncloud layer emphasize that it is only the cloud layer that is particularly influenced by the broadband parameterization.

The fluxes absorbed above, in, and below the cloud, and the corresponding absolute errors are shown for clouds at a high (180–200 mbar) and a low (900–920 mbar) location in Figures 15 and 16, respectively, as a function of drop optical depth. The absorption by the above-cloud and the below-cloud vapor, and by the cloud itself, vary monotonically with optical depth. For the high cloud case (Figure 15), there is an anticorrelation between the in-cloud and the below-cloud absorption, with very little contribution from the above-cloud vapor. This case yields differences in the absorption below the cloud of 20 W/m^2, indicating that broadband corrections for vapor above and in cloud, which have been the focus of this study, do not necessarily imply a high accuracy for the below-cloud vapor absorption. For the low cloud case (Figure 16) the above-cloud vapor absorption is the dominant contributor to the atmospheric absorption, increasing as drop optical depth and, hence, as the reflected flux at the cloud top increases. In-cloud absorption is also significant at the larger optical depths and, although following the same pattern of increase with optical depth as in Figure 15, is less in magnitude than in the high cloud case. This underscores the impact of the above-cloud vapor on the actual flux absorbed by cloud drops [*Davies et al.*, 1984; RF]. Errors are generally much smaller in Figure 16 than for the high-cloud case (<6 W/m^2).

It may be expected from Figure 15 that the relative errors in the surface flux would be large for the high cloud case. This is shown in Figure 17 together with the reference values; the latter exhibit a monotonic decrease with increase in the high cloud drop optical depth. The relative error increases with optical depth (~12% for τ_{drop} = 100); the absolute errors, however, become smaller. Table 7 lists the absolute errors for the high and the low cloud cases of various optical depths, and for 3 sun angles. As with heating rates, the largest absolute errors (~17 W/m^2) occur for optical depths ~10 and overhead sun. The absolute errors in the surface fluxes when the cloud is located at lower altitudes (see Table 7) are smaller (<2 W/m^2) compared to the high cloud case.

Table 7 also lists the absolute errors in the top of the atmosphere reflected flux. These are less than 8 W/m^2 and correspond to relative errors of <5%. The larger values occur for the low clouds with large drop optical depths. The values for the high cloud cases are indicative of the errors that arise principally due to the uncertainties in the representation of $\bar{R}_0$ and $\bar{T}_0$. Again, errors at normal incidence are a good representation of the maximum absolute errors. The low absolute error values confirm the validity of the assumption that the reflected flux is virtually independent of the in-cloud vapor for the 20-mbar cases.

5.2. *Miscellaneous Tests*

Next, the errors are investigated for cases when the overcast sky parameters are different from those considered above. Our inspection of the results for the tropical and the

TABLE 6. Absolute Error in the Heating Rate of a 1-Layer CS Cloud of Specified Drop Optical Depth τ_{drop} Located at a High (180–200 mbar) or a Low (900–920 mbar) Altitude, for Solar Zenith Angles Θ_0 of 0°, 53°, and 75° (see Section 5.1)

	Θ_0 = 0°		Θ_0 = 53°		Θ_0 = 75°	
	High	Low	High	Low	High	Low
τ_{drop} = 1		−1.0		−0.1		0.5
τ_{drop} = 5		−1.7		−0.7		−0.1
τ_{drop} = 10		−2.3		−1.1		−0.3
τ_{drop} = 50		−1.1		−1.1		−0.7
τ_{drop} = 100		0.6		−0.4		−0.6

Values are in kelvins per day. The reference values and the relative errors appear in Figures 11–13. The corresponding flux value (in watts per square meter) is 2.4 times the heating rate for the model structure assumed in the present study. Solar irradiance for overhead sun at the top of the atmosphere over the spectral interval considered is 966 W/m^2.

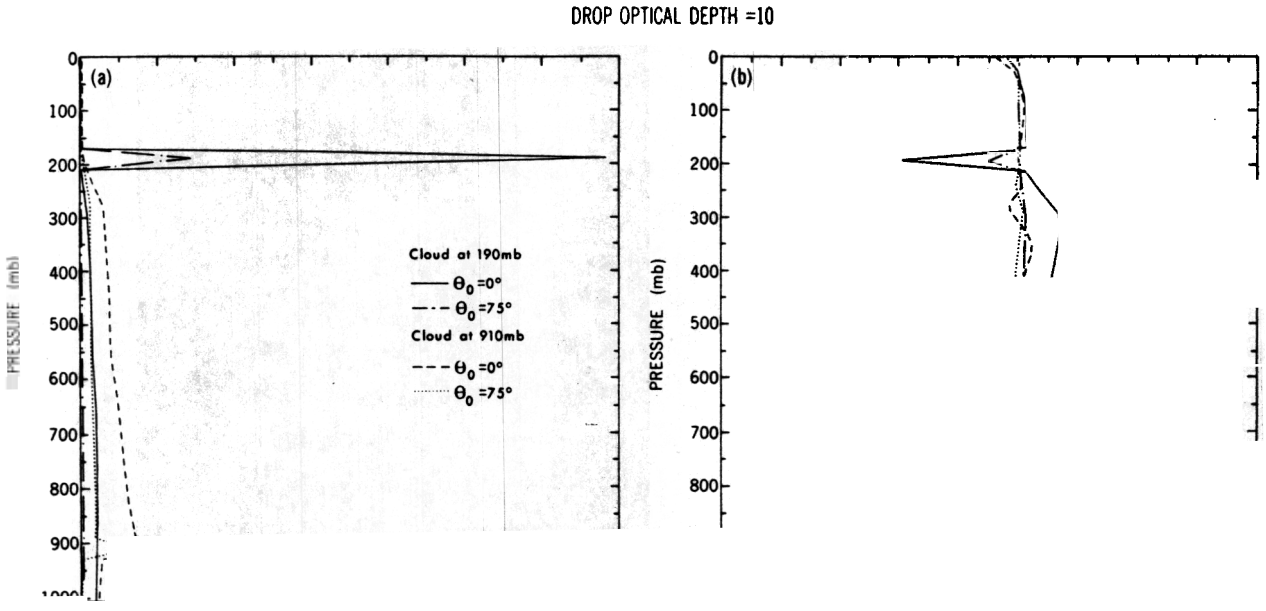

sub-Arctic winter atmospheric profiles [*McClatchey et al.*, 1972] show these to be only slightly less accurate than for the mid-latitude summer profile.

We next examine the errors for drop optical depths that lie outside the range (1–100) used in constructing the parameterization (equations (21) and (22); section 4.3). Note that the largest errors can be expected to occur for low clouds. For overhead sun and CS clouds with drop optical depths of 0.5 or 200 and located in the layer 900–920 mbar, the errors are less than 20% for heating rate and less than 5% for fluxes. The relative errors are larger for these cases than for the optical depth range 1–100; however, these errors are still less than the maximum values seen in Figure 11.

Because there is a substantial range possible in the values of some other parameters that can affect the transfer in cloudy atmospheres, only a few examples are considered here. The choices are guided by the results obtained in section 5.1 (Figures 11–17); Tables 6 and 7), and by the intent to estimate the maximum possible errors. Accordingly, only the results for low clouds with drop optical depths of 10 or 100 are discussed below.

Extended (geometrically thicker) clouds. Clouds that are more than 20 mbar thick contain more water vapor than those considered so far. This suggests a more important role for the in-cloud vapor. For example, if extended clouds spanning the levels 800–900 mbar, 600–900 mbar, and 300–800 mbar in a mid-latitude summer atmosphere are considered, the water vapor amounts inside these systems corresponding to saturation conditions can be substantially higher than in the 900- to 920-mbar and 180- to 200-mbar systems (Table 8). In this regard, the 20-mbar clouds may be considered to be the limit when drops are present with the least amount of in-cloud vapor. The parameterization recipe outlined at the beginning of this section is adapted to the extended systems by considering the entire cloud to comprise one layer, with drops and the total in-cloud vapor forming separate sublayers, as stated in section 4.5.

The absolute and the relative errors due to the present broadband treatment for the various cloud systems are listed in Table 9 for 0° incidence. The departures from the reference results increase with water vapor content, suggesting a deficiency in the treatment of the vapor-drop interactions inside the cloud. The absolute errors in the absorbed flux reach 36 W/m^2 when τ_{drop} = 10 and ~28 W/m^2 when τ_{drop} = 100 for the 600- to 900-mbar system; the relative errors are <24%.

For τ_{drop} = 1, the absolute and relative errors (<10%) become smaller (not shown) because the cases begin to resemble more the vapor-only situation and the drops have a less important role. Note that in the limit that the drop optical depth becomes $\ll$1, the cloud transmission can be expected to be well simulated according to the results of section 2.

The results for 75° incidence also exhibit more error (not shown) for the thicker systems. The underestimate in the absorption due to in-cloud vapor and the obvious increase in the importance of this effect with increasing slant vapor path yields a relative error of −29% for the τ_{drop} = 10, 600- to 900-mbar case; as was noted before, absolute errors are less than for the 0° incidence.

These results highlight the importance of water vapor inside geometrically thick clouds, an issue that has sometimes been relegated as unimportant and whose quantitative significance has not been declared explicitly in past studies. For clouds that are up to 100 mbar thick in the lower troposphere, accounting for the attenuation of water vapor above the cloud is a principal consideration in providing a good approximation to the flux disposition in the atmosphere. For thicker geometrical extents and increasing in-cloud vapor, the broadband treatment does not adequately represent the spectrally dependent multiple-scattering process involving drops and vapor, leading to heating rate underestimates.

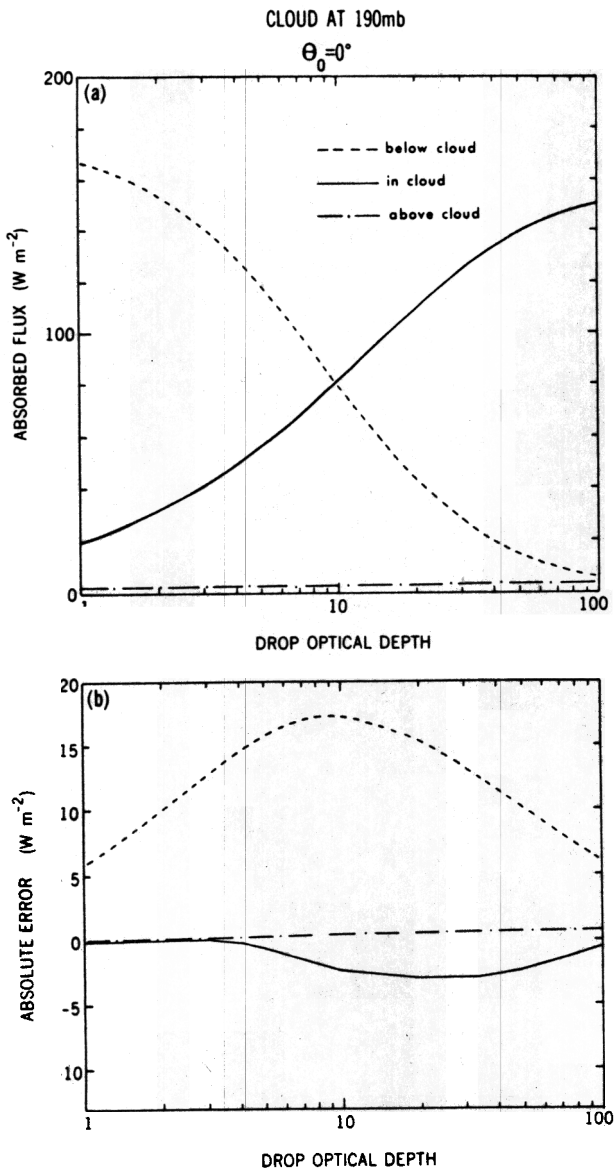

Fig. 15. (*a*) Reference values of the fluxes absorbed above, in, and below CS clouds of various drop optical depths located at 180–200 mbar and illuminated by the overhead sun. (*b*) Absolute errors due to the new parameterization.

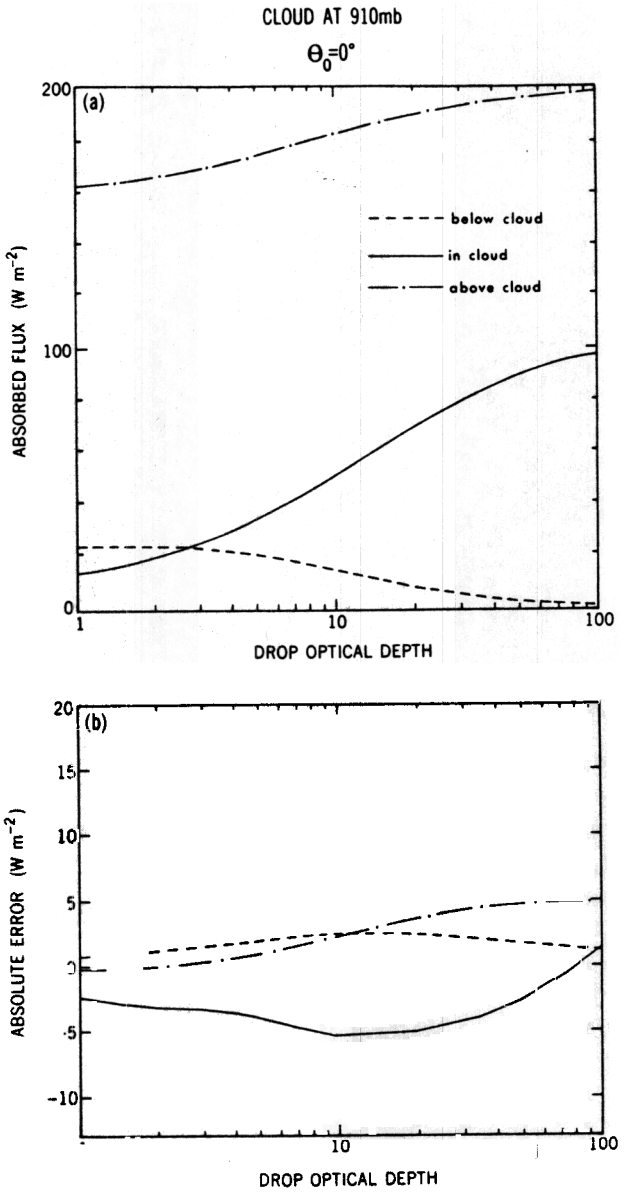

Fig. 16. Same as for Figure 15, except for a CS cloud located at 900–920 mbar.

The relative error in the reflected flux at the top of the atmosphere (Table 9) is not as sensitive (~2% or less) to the cloud thickness as the absorbed flux. Thus despite the increased vapor content in the extended systems, the approximations concerning the cloud reflection do not enhance the relative errors in the atmospheric albedo, substantiating the effect noted for the 20-mbar-thick clouds in Table 7, and emphasizing the adequacy of the assumptions in section 4.5. The absolute errors (up to 16 W/m^2), however, show an increase from those for the 20-mbar clouds. Tests with high clouds (not shown) indicate that the absolute errors in the surface flux for thicker (>20 mbar) systems are less than for the 20-mbar case (Table 7); this is true for the relative error, too (<5%).

CL cloud model. The ICRCCM CL cloud model contains larger drops and therefore has lower single-scattering albedos across the spectrum than does the CS cloud (Table 3). The errors for the four cloud systems are listed in Table 9. The heating rate errors are less than for the CS cloud, even for extended systems (e.g., 300–800 mbar). This is because, relative to the CS cases, a greater proportion of the absorption inside the CL cloud is by drops rather than by vapor, leading to a constrained importance for the latter. For high clouds (not shown), the errors in the surface flux are larger than for the CS cases, reaching 30 W/m^2, although the relative errors are again <10%. From the CS and the CL cloud results, it is concluded that the reflected flux is well simulated under all circumstances; however, the surface flux can attain large absolute errors.

6. Comparison of Various Broadband Treatments

In this section, a comparison is made of the accuracies of different broadband treatments of vapor-drop interactions that have been considered for or used in GCM studies, including the parameterization employed in section 5.

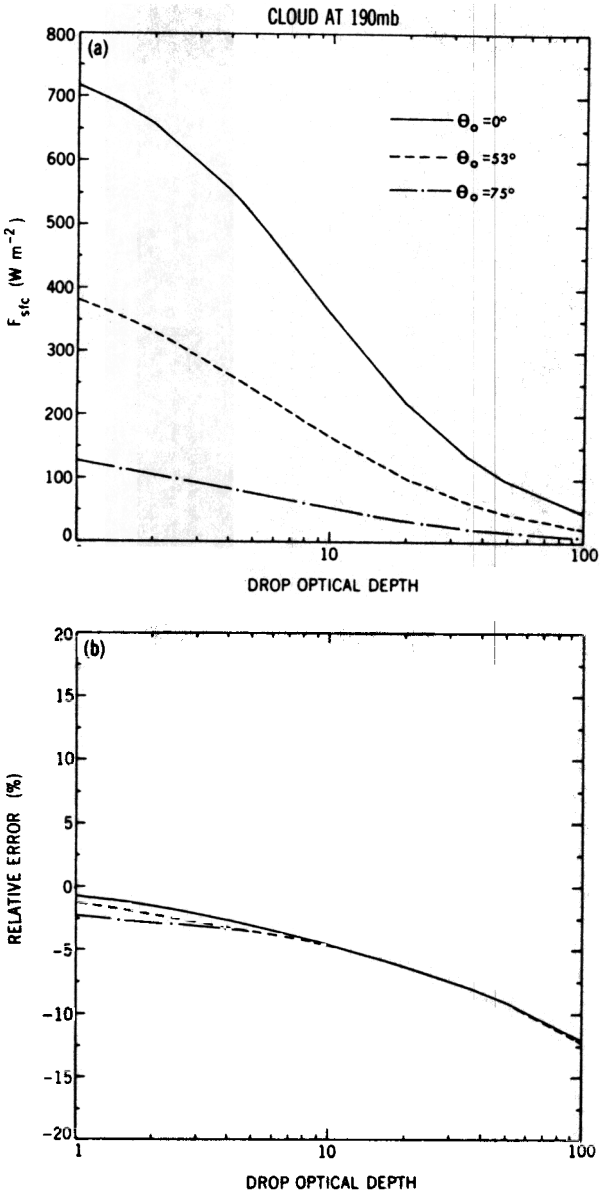

Fig. 17. (*a*) Reference values of the flux reaching the surface (F_{sfc}) in overcast atmospheres containing a CS cloud at 180–200 mbar of different drop optical depths. Three different sun angles Θ_0 are considered. (*b*) Relative errors due to the new parameterization.

6.1. *"Mean" Drop Single-Scattering Properties*

As was stated in section 4.2, one way to derive broadband drop radiative properties is to specify some spectral "mean" value for the drop single-scattering properties [LH; *Harshvardhan et al.*, 1987; *Charlock and Ramanathan*, 1985]. The cloud layer reflection and transmission and the flux disposition can then be obtained by employing the *Harshvardhan et al.* [1987] method, except using the modified LH water vapor absorption scheme. A subset of this approach is to assume that drop absorption is negligible [LH] or to ignore it [*Chou and Arking*, 1981]. The effects due to such assumptions are investigated for 20-mbar CS clouds of different drop optical depths (1–100) and located at different altitudes (100–1000 mbar). The relative errors in the cloud layer heating rates are shown in Figure 18 for the overhead sun case. Three different values of the broadband drop single-scattering albedo ω are considered. The assumption of no absorption by the drops (ω of drops = 1) leads to large underestimates of the cloud heating (>40%) and is obviously an unreasonable assumption. For $\omega < 1$, a fair agreement can be found over a certain range of parameters, e.g., when $\omega = 0.999$, and $\tau < 2$ or $\tau > 25$, errors can be <20%; the agreement is poorer otherwise and errors can be as high as 40%. The results of Figure 18 indicate that it is not possible to assign a single ω value for drops that would ensure uniformly accurate results for cloud absorption over the range of overcast atmospheres considered.

TABLE 7. Absolute Error in the Fluxes (W/m^2) at the Surface and That at the Top of the Atmosphere for a CS Cloud of Specified Drop Optical Depth (τ_{drop}), Located at a High (180–200 mb) or a Low, (900–920 mbar) Altitude, for Solar Zenith Angles Θ_0 of 0°, 53°, and 75° (see Section 5.1)

	Θ_0 = 0°		Θ_0 = 53°		Θ_0 = 75°	
	High	Low	High	Low	High	Low
Downward Flux at Surface						
τ_{drop} = 1	−5.9	1.3	−5.2	−0.4	−3.0	−0.7
τ_{drop} = 5	−16.1	−1.1	−8.6	−0.3	−2.7	0.3
τ_{drop} = 10	−16.5	−1.1	−7.7	0.4	−2.4	0.4
τ_{drop} = 50	−8.6	0.5	−3.9	0.5	−1.2	0.3
τ_{drop} = 100	−5.6	0.1	−2.6	0.2	−0.8	0.1
Reflected Flux at Top of Atmosphere						
τ_{drop} = 1	−0.1	0.6	0.1	0.4	0.1	−0.1
τ_{drop} = 5	0.4	2.1	0.2	0.9	0.1	0.1
τ_{drop} = 10	0.8	1.5	0.3	0.7	0.2	0.6
τ_{drop} = 50	−0.1	−4.7	0.1	0.1	0.2	1.6
τ_{drop} = 100	−0.8	−7.9	−0.2	−1.1	0.2	1.4

Values are in watts per square meter. The solar irradiance for overhead sun at the top of the atmosphere over the spectral interval considered is 966 W/m^2.

6.2. *"Mean" Drop Reflection and Transmission*

As was already demonstrated in this study, it is possible to define the drop reflection and transmission for each spectral interval using the spectrally dependent drop single-scattering parameters, and then perform an average (equations (15) and (16) or (17) and (18)) to obtain the "mean" spectral reflection and transmission. Over the years, various studies have used this concept in different ways. The impacts of the various techniques on the accuracy of the simulated results is explored below.

In contrast to the ICRCCM drop models used in section 5, we consider here a formalism developed by *Slingo* [1989]. This is an attractive representation of drop spectral single-scattering properties in terms of two parameters, liquid water path and effective radius of the drop distribution. We

TABLE 8. Water Vapor Amount Corresponding to Saturation Conditions Within Clouds and Spanning the Pressure Levels Indicated in a Mid-Latitude Summer Atmosphere

Cloud Location, mbar	Water Vapor Amount, kg/m^2
180–200	0.006
900–920	2.47
800–900	10.4
600–900	21.79
300–800	15.37

9. Absolute and Relative Errors in the Flux Absorbed Within Cloud Layers for the Miscellaneous Cases Discussed in Section 5.2

	ΔF_{abs}				ΔF_{TOA}			
	τ_{drop} = 10		τ_{drop} = 100		τ_{drop} = 10		τ_{drop} = 100	
Case	Absolute, W/m^2	Relative, %	Absolute, W/m^2	Relative, %	Absolute, W/m^2	Relative, %	Absolute, W/m^2	Relative, %
				CS (Mid-Latitude Summer)				
900–920 mbar	−5	−10	1	1	1	1	−8	−1
800–900 mbar	−16	−18	−12	−11	2	1	0	0
600–900 mbar	−36	−24	−28	−18	8	2	13	2
300–800 mbar	−35	−19	−23	−13	10	2	16	2
				CL (Mid-Latitude Summer)				
900–920 mbar	2	2	8	5	−3	−1	−14	−2
800–900 mbar	−2	−2	−4	−2	−5	−2	−7	−1
600–900 mbar	−14	−7	−15	−6	−4	−1	2	1
300–800 mbar	−9	−4	−9	−4	−3	−1	6	1

The results are for the broadband parameterization developed here as compared with the reference calculations. Select CS and CL model cloud cases for overhead sun are considered, with drop optical depths (τ_{drop}) of 10 or 100. In-cloud water vapor amounts are listed in Table 8. Only the errors in the absorbed (ΔF_{abs}) cloud fluxes and in the reflected fluxes at the top of the atmosphere (ΔF_{TOA}) are listed.

use here the higher spectral resolution table from *Slingo* [1989], although the results would apply equally well to his coarser tabulations. First, a set of reference results (section 3) are determined corresponding to the spectrally dependent single-scattering parameters. Then we investigate the consequences of applying four different broadband techniques A–D, as described below, to compute the cloud layer radiative properties and the resultant fluxes. The methodology for each technique is the same as outlined at the beginning of section 5 (steps 1–7), except that step 1 now is based on the Slingo table; other exceptions and modifications are as noted:

Technique A. Cloud layer properties are represented by $\bar{R}_0$ and $\bar{T}_0$, as in (15) and (16); this effectively ignores the influences due to both the above-cloud and the in-cloud vapor absorption on the broadband drop reflection and transmission values.

Technique B. Technique B is the same as A, except accounting for in-cloud vapor absorption in the manner described in section 4.5. This method, like A, also ignores the effect of the above-cloud vapor on the broadband drop radiative properties [e.g., *Wetherald and Manabe*, 1988].

Technique C. This technique is the same as B, except increasing the vapor path inside the cloud by a factor of 5 to account approximately for the enhancements due to multiple scattering by droplets [*Ramanathan et al.*, 1983]; this concept has its origins in the work of *Sasamori et al.* [1972].

Technique D. Cloud radiative properties are adjusted for the influences due to the above- and in-cloud vapor, as in section 5; for the former effect, the equations for $\bar{R}_l/\bar{R}_0$ and $\bar{T}_l/\bar{T}_0$, as applicable for CS drops (Table 4), are employed. This assumes that the variation with height of (19) and (20) for the Slingo model is represented adequately by the parameterization for the CS model (equations (21) and (22)).

It is noted that while Slingo's study implies method A, it suggests adopting method C for GCM applications. Also, it is necessary to make one more modification in order to use the modified LH vapor absorption scheme (section 2) along with the broadband Slingo drop model. The former is derived for the spectral range 0–18,000 cm^{-1} while the Slingo table terminates at 2500 cm^{-1}. For the sake of completeness, the values corresponding to the CS drop single-scattering parameters (first interval in Table 3) are used below 2500 cm^{-1}. The total incident solar flux at the top of the atmosphere is small for this highly absorbing band (14 W/m^2), so that the principal conclusions are unaffected by this modification.

The four cloud systems employed in section 5 (900–920, 800–900, 600–900, and 300–800 mbar) are considered again to intercompare the techniques A–D. The results are analyzed with respect to three different parameters: drop optical depth (10 or 100), effective radius (r_e = 5 or 15 μm), and solar zenith angles (0° or 75°). For r_e = 15 μm, the two optical depths correspond to liquid water paths of ~87 and 870 g/m^2, respectively. The absorbed flux by the cloud and the relative influence of the vapor on the convergence in the cloud layer (computed in the same manner as for Figure 10) are listed in Table 10 for the four cloud systems, with the in-cloud vapor specified as in Table 8. The absorbed flux and the importance of the in-cloud vapor vis-à-vis drops increases substantially for the thicker cloud systems which contain larger amounts of water vapor. The larger effective radius case possesses a higher drop absorption optical depth so that the relative effect of the in-cloud vapor is less than that for the 5-μm case. The higher zenith angle has less flux incident at the top so that the absolute values of the absorbed flux in the cloud are lower than for the overhead sun; however, the trends with respect to increase in in-cloud vapor and with drop size remain qualitatively similar.

The focus is again confined to the simulation of the flux convergence in the clouds by the various techniques. The relative errors in the results from the various techniques, when compared to the appropriate reference values, are listed in Table 11 for overhead sun and for all the parameter values considered in Table 10. It is apparent that each technique can be superior to the others over definite ranges in the in-cloud vapor content. All the techniques have a tendency to yield lesser absorption than the reference values with increasing in-cloud vapor.

Consider the results for r_e = 5 μm. Since technique A ignores the effect of the above-cloud vapor on the cloud layer reflection and transmission values, this would, by

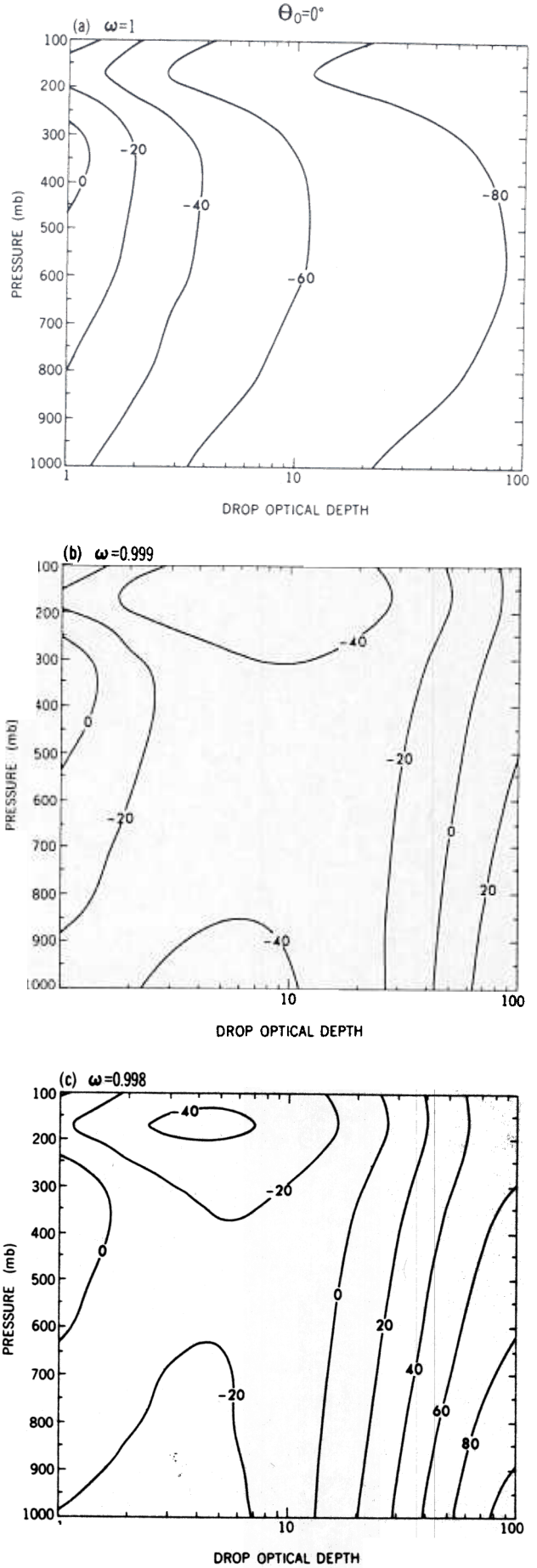

TABLE 10. Reference Computations of the Absorbed Flux in Clouds Using *Slingo's* [1989] Single-Scattering Parameters, and the Relative Effect of in-Cloud Vapor on the Cloud Layer Absorption, as Obtained for Four Cloud Systems of Different Pressure Thicknesses (Section 6.2)

	$\Theta_0 = 0°$		$\Theta_0 = 75°$	
Case	Flux, W/m^2	Vapor Effect, %	Flux, W/m^2	Vapor Effect, %
	$\tau_{drop} = 10$; $r_e = 5$ μm			
900–920 mbar	47.65	25	6.77	15
800–900 mbar	85.15	53	11.29	41
600–900 mbar	154.04	68	23.38	62
300–800 mbar	190.37	64	33.88	59
	$\tau_{drop} = 100$; $r_e = 5$ μm			
900–920 mbar	91.77	8	12.14	4
800–900 mbar	117.06	22	15.20	15
600–900 mbar	156.53	30	21.79	24
300–800 mbar	176.95	21	28.90	19
	$\tau_{drop} = 10$; $r_e = 15$ μm			
900–920 mbar	71.85	15	12.44	8
800–900 mbar	107.66	38	17.20	26
600–900 mbar	178.66	54	30.52	47
300–800 mbar	221.17	52	42.85	46
	$\tau_{drop} = 100$; $r_e = 15$ μm			
900–920 mbar	143.09	5	20.56	2
800–900 mbar	169.43	13	24.13	8
600–900 mbar	212.44	19	32.00	15
300–800 mbar	241.64	12	41.51	11

Drop optical depths (τ_{drop}) of 10 and 100, and effective radius (r_e) of 5 and 15 μm are considered; the in-cloud water vapor amounts are listed in Table 8. Solar zenith angles Θ_0 considered are 0° and 75°. The total near-infared solar irradiance at the top of the atmosphere for overhead sun is 960 W/m^2.

itself, cause an overestimate in the absorbed flux. As the technique also ignores the in-cloud vapor, this, in contrast, would yield an underestimate in the absorption. The net effect of these two mechanisms is to cause an overestimate for relatively thin systems when the in-cloud vapor amount is small, and an increasing underestimate as vapor contents become large.

Compared to A, B yields more absorption leading to larger overestimates for the lower vapor content case (900–920 mbar) and lesser underestimates for the higher in-cloud vapor content cases. Technique C, which considers an arbitrary increase in the in-cloud vapor optical depth, is a somewhat exaggerated version of B. It proves to be the most accurate for the geometrically thicker systems but can yield large overestimates (~50%) for systems that are ~100 mbar thick.

The results of technique D ($r_e = 5$ μm) bear a close resemblance to the trends seen for the CS cloud in section 5, suggesting that the application of the CS model parameterizations of $\bar{R}/\bar{R}_0$ and $\bar{T}/\bar{T}_0$ (Table 4) to this Slingo model is acceptable. The absorbed flux for the 900- to 920-mbar system is more accurate with D than with any other method.

Fig. 18. (Opposite) Errors (percent) in the heating rate within 20-mbar-thick CS clouds, as a function of drop optical depth and altitude (solar zenith angle $\Theta_0 = 0°$). Broadband drop single-scattering albedos ω of (*a*) 1 (i.e., no drop absorption), (*b*) 0.999, and (*c*) 0.998 are considered (see section 6.1).

TABLE 11. Relative Errors in the Absorbed Flux Within Cloud Layers Due to Different Treatments of Broadband Vapor-Drop Interactions for Overhead Solar Incidence

Case	Relative Error Due to Technique, %			
	A	*B*	*C*	*D*
	$\tau_{drop} = 10; r_e = 5\ \mu m$			
900–920 mbar	31	44	79	−10
800–900 mbar	−24	7	51	−19
600–900 mbar	−55	−15	16	−25
300–800 mbar	−61	−18	6	−21
	$\tau_{drop} = 100; r_e = 5\ \mu m$			
900–920 mbar	36	37	39	3
800–900 mbar	10	13	17	−10
600–900 mbar	−12	−7	−3	−19
300–800 mbar	−17	−11	−8	−15
	$\tau_{drop} = 10; r_e = 15\ \mu m$			
900–920 mbar	33	42	68	6
800–900 mbar	−8	19	57	−2
600–900 mbar	−41	−3	27	−11
300–800 mbar	−49	−8	15	−10
	$\tau_{drop} = 100; r_e = 15\ \mu m$			
900–920 mbar	31	32	34	12
800–900 mbar	15	17	20	2
600–900 mbar	−3		5	−6
300–800 mbar	−8	−3	−1	−6

The drop single-scattering properties follow *Slingo's* [1989] formulation. Four different broadband techniques *A*, *B*, *C*, and *D* (present parameterization), as described in section 6.2, are employed. The cloud cases considered correspond to those listed in Table 10.

However, B provides a better result with respect to the reference results for extended systems that contain more vapor than the 900- to 920-mbar cloud.

In actuality, both B and D, and, for that matter, all the techniques, represent the broadband in-cloud vapor and drop interactions poorly and yield an underestimate in the cloud absorption. However, B makes a deliberate overestimate of the radiation incident on cloud top by considering equations (15) and (16), instead of (17) and (18). This allows more radiation to be absorbed by the drop in the parameterization, thus partially correcting for the underestimate due to the in-cloud vapor absorption. This is made evident when the accuracies of B and D are compared for the 600- to 900-mbar case. The difference between the two cases (−15% versus −25%) is a measure of the overestimate caused by the absence of considerations for the above-cloud vapor. Note also that B has more of an underestimate for the 300- to 800-mbar system than for the 600- to 900-mbar system even though the vapor content in the latter is larger. This is because the above-cloud vapor is less in the 300- to 800-mbar case, introducing less of an overestimate in the drop absorption; thus the underestimate due to in-cloud vapor absorption is not offset by the overestimate in the drop absorption for the 300- to 800-mbar case as much as for the 600- to 900-mbar system. B thus represents an interesting quirk inasmuch as two errors of opposite signs compensate partially, improving the end result. The importance of including in-cloud vapor effects is emphasized when B and D are compared with A.

The errors in Table 11 indicate that D is more accurate at the larger optical depths, consistent with Figure 11. This is because at the higher optical depth there is a decreased importance of the in-cloud vapor relative to droplets (Figure 10). Also, the relative errors due to the above-cloud vapor effect become small. These features also affect B and C for the $\tau_{drop} = 100$ case, yielding a smaller overestimate due to ignoring the above-cloud vapor effect for the 900- to 920-mbar system, and a smaller underestimate due to the in-cloud vapor effect for the 600- to 900-mbar system.

The results for the larger effective radius ($r_e = 15\ \mu m$) in Table 11 exhibit trends similar to those mentioned for the smaller r_e. Because larger drop sizes imply a lesser single-scattering albedo for the same drop optical depth, the importance of in-cloud vapor absorption relative to cloud drop absorption diminishes (Table 10). Because of the decreased importance of the in-cloud vapor, A, B, and C, when applied to the extended systems, yield larger overestimates (or lesser underestimates) for the 15-μm effective radius than for the smaller size.

Turning to the results for the boundary fluxes (not shown), the maximum absolute error in the reflected flux at the top of the atmosphere for any of the cases in Table 11 with technique D is 26 W/m^2, being higher than for the CS drop model (Table 9). The relative errors continue to be small (<4%). For A, B, and C, the maximum absolute error is −32 W/m^2 (relative error −6%), being the same for all three since the above-cloud vapor effects on the cloud albedo are ignored in each.

For overhead sun, the maximum absolute error in the surface flux for D is 21 W/m^2, with the maximum relative error being 7%. These values are approximately similar to the maximum values discussed in section 5. For B, the maximum absolute error is 19 W/m^2 and the worst relative error is −9%. For A and C the magnitude of the error can exceed 26 W/m^2, while the worst relative error is −16%. The errors in the absorbed flux by the water vapor in the rest of the atmosphere are much less than the errors in the cloud absorption, even lower than that in the boundary fluxes.

Relative errors for the cloud systems at a high solar zenith angle (75°) are listed for the four broadband techniques in Table 12. The absolute values of the fluxes and the maximum absolute errors are smaller than for the 0° zenith angle. Because the vapor path length above the cloud is larger at the higher zenith angle, techniques A, B, and C, which have no provision to treat this effect, are degraded more in their accuracies, particularly when the cloud system is not thick. Errors >35% can occur with B even for 100-mbar-thick systems. While D treats the above-cloud slant path in a better fashion, it, just like the others, cannot treat adequately the effect of the vapor + drop interactions within the cloud. Thus errors due to the inadequacies in treating the in-cloud vapor and drop interactions persist at the higher zenith angle for all methods. Relative errors for larger optical depths and for the larger effective radius are also more severe for A, B, and C at the 75° incidence than at 0°. The maximum relative errors in the boundary fluxes increase for all techniques at the higher zenith angle. For D this value is 14%, but it is accompanied by small absolute values.

From the preceding discussions, techniques A and C yield less satisfactory results in general than B and D. Across the range of the vapor contents considered, both B and D are degraded for the higher vapor content cases, B less than D owing to a cancellation of errors of opposite signs. Method D is necessarily biased toward good simulations for 20-mbar-

TABLE 12. Same as Table 11, Except for a Solar Zenith Angle of 75°.

Case	Relative Error Due to Technique, %			
	A	*B*	*C*	*D*
	$\tau_{drop} = 10; r_e = 5\ \mu m$			
900–920 mbar	86	91	109	−8
800–900 mbar	17	34	71	−23
600–900 mbar	−38	−10	19	−31
300–800 mbar	−53	−20	0	−26
	$\tau_{drop} = 100; r_e = 5\ \mu m$			
900–920 mbar	70	70	71	−7
800–900 mbar	42	43	47	−17
600–900 mbar	8	12	16	−21
300–800 mbar	−10	−5	−2	−14
	$\tau_{drop} = 10; r_e = 15\ \mu m$			
900–920 mbar	66	69	79	15
800–900 mbar	25	38	65	
600–900 mbar	−23	1	26	−15
300–800 mbar	−39	−10	7	−15
	$\tau_{drop} = 100; r_e = 15\ \mu m$			
900–920 mbar	55	55	56	12
800–900 mbar	38	40	42	4
600–900 mbar	14	17	20	−4
300–800 mbar	−3	1	3	−5

thick systems, in view of its derivation from reference results that employ vapor absorption coefficients defined for 20-mbar layers.

Considering all the cases examined here, both techniques B and D incur errors of up to 40 W/m^2 in cloud absorption and about 30 W/m^2 or less in the fluxes at the atmospheric boundaries. In general, for cloud tops located at higher altitudes than shown in the tables, the errors for A, B, and C would be smaller. D would yield smaller errors for systems located at the altitudes considered in Tables 11 and 12 but having lesser vapor amounts. The accuracy of methods that do not account for the influence of the above-cloud vapor on the drop radiative properties are degraded considerably when the vapor contents in cloud are small and when the drop effects are relatively large. Conversely, when the in-cloud vapor increases to larger amounts, all methods underestimate the increase in cloud absorption.

As a final point, we consider the parameterization of cloud layer reflection and transmission of *Stephens et al.* [1984]. Here the above-cloud and the in-cloud vapor effects are incorporated implicitly in the parameterization by performing detailed computations for a number of model clouds placed at specific locations in the model atmosphere. Computations according to this method, with $\tau_{drop} = 10$ and effective radii of 5 and 15 μm, yield cloud absorption, respectively, of ~111 and 159 W/m^2 (normal incidence). Considering Table 10, these values are intermediate between the results for the four systems. However, it is evident that owing to the lack of an explicit functional dependence on the above-cloud vapor path and the amount of the in-cloud vapor, the results from this method cannot be expected to be accurate over all of the parameter space covered in Table 10. A similar conclusion also applies to the approach of prescribing broadband "mean" drop single-scattering properties described at the beginning of this section.

7. General Overcast Sky Considerations

Thus far, the analysis has dealt with the critical issues concerning the broadband parameterization in the context of single cloud decks above a nonreflecting surface. The applicability of the broadband concept to arbitrary overcast skies requires an investigation into two additional types of problems that are considerably more complex, namely, clouds over reflecting surfaces and multiple cloud decks located at different altitudes. A detailed examination of these problems is beyond the scope of this study. However, we have analyzed broadband results for a limited number of these types of cases. We use these to summarize the conceptual difficulties and the worst inaccuracies arising when the broadband treatment is extended to general overcast atmospheres.

In order to illustrate the issues involved, we consider two specific instances. One is when high clouds occur above a highly reflecting surface, while the other is when a low thick cloud is present beneath a high cloud. Now, interactions of any cloud with the diffuse beam as well as multiple reflections with other clouds and/or surface must be considered. In the broadband framework, the parameterization of the spectrally dependent optical path traversed by the direct and diffuse beams through both water vapor and drops, including obtaining an account due to multiple reflections, constitutes the principal obstacle. In both instances, although it is certain that R_0 and T_0 (equations (15) and (16)) cannot be applied to the cloud layer(s) with rigor (section 4.3), it is a daunting task to determine the relevant R and T (analogous to (17) and (18)) in a general manner. This is to be contrasted with the single cloud deck case where it is possible to estimate relatively simply the vapor optical path above the cloud (equation (23)) and thus obtain the appropriate broadband R and T (equations (21) and (22)).

Notwithstanding these difficulties and in order to retain the broadband concept for all types of overcast atmospheres, we suggest a simple albeit crude addition to the prescription already outlined for single cloud decks over a nonreflecting surface (see beginning of section 5; steps 1–7):

1. The reflectivity and transmissivity of the highest cloud to the direct beam are computed as before, i.e., using (21) and (22) and employing the formulation developed in this study (section 4), while the corresponding quantities for all other clouds follow (15) and (16).

2. The diffuse quantities R^f and T^f for all clouds are assumed to be the same as R^f_0 and T^f_0 (defined analogous to (15) and (16), except for a diffuse beam incident on the cloud, indicated by superscript f, and assumed to be isotropic [*Coakley et al.*, 1983]).

We explore the numerical consequences of these assumptions for the two instances cited, using, as in section 6, the Slingo drop properties ($r_e = 5\ \mu m$) and considering overhead sun. Multiple reflections at every frequency in the LBL + DE reference and in each pseudo-monochromatic interval (Table 2) in the broadband calculations are treated following *Coakley et al.* [1983].

First, consider a high cloud (optical depth 10, located at 180–200 mbar) over a highly reflecting surface (Lambertian surface with an albedo of 0.8). In this case, the absolute (relative) error in the surface flux is −34 W/m^2 (−6%), while that in the absorbed flux is 22 W/m^2 (26%). For optical depths of 1 and 100, the errors are less. Smaller errors occur

in the top-of-the-atmosphere reflected flux. The errors in the transmitted flux at the surface and in the cloud absorption are greater than for the corresponding nonreflecting surface cases in section 5. However, these errors are less than the worst inaccuracies noted in sections 5 and 6.2 (see technique D).

Next, consider a high cloud (180–200 mbar) of optical depth 1 overlying a low (800–900 mbar), thick cloud of optical depth 100. In this case, the error in the high cloud heating is 10 W/m^2 (50%) while that for the low cloud is 25 W/m^2 (24%). The reflected flux at the top is in error by −32 W/m^2 (−5%). If the high cloud optical depth is 10, the errors in the heating become 29 W/m^2 (34%) for the high cloud and 39 W/m^2 (76%) for the low cloud. In this case, the reflected flux at the top is in error by −66 W/m^2 (−10%). Surface flux errors are less than 10 W/m^2 (~20%) in magnitude.

Compared to the maximum errors in cloud absorption for the cases studied in sections 5 and 6.2 (see technique D), these results, although exhibiting larger relative values, yield approximately similar or less absolute flux errors. The absolute error in the reflected flux at the top of the atmosphere, as seen in the second example, can be considerable while the large relative errors in the surface fluxes tend to be accompanied by small absolute values. Otherwise, the errors in the fluxes at the boundaries of the atmosphere are less than ~10%, which is somewhat greater than for the single cloud deck cases in the earlier sections. Note that the cloud heating is overestimated while the reflected flux is underestimated.

Although the investigations concerning arbitrary overcast sky cases here are not exhaustive, the above examples indicate that, with exceptions, the broadband parameterization for a single cloud deck can be generalized with errors not too dissimilar to the maximum values appearing in sections 5 and 6. The exceptions, however, lead to the conclusion that the present broadband treatment of the drop + vapor interaction with solar radiation needs to undergo further refinements in order to be more accurate for all types of overcast atmospheres. It is important to point out that similar or larger inaccuracies prevail for the above problems no matter which type of broadband method of section 6 is employed. These considerations suggest that the broadband methods may be more limited in their accuracy than was previously thought, especially for skies with multiple cloud decks. Thus broadband methods should be used in a GCM with the realization that in some cases, the results could become more inaccurate than is desired for the problem under investigation.

8. Summary and Conclusions

Using reference solutions determined for a variety of atmospheric conditions, this study has investigated the accuracy of broadband (i.e., use of one effective spectral interval) treatments of the near-infrared radiative interactions in atmospheres containing water vapor and water drops. Such broadband treatments are necessitated when the optical properties of at least one of the constituents are available only for the near-infrared spectrum as a whole. For the problem of solar absorption by water vapor, the accuracy of two broadband methods employed in current GCMs is evaluated. Both methods yield an underestimate in absorption. Corrections are introduced in one of them, leading to the modified Lacis-Hansen technique (section 2). This modified method yields excellent simulations of the solar flux convergences in clear skies.

In order to highlight the critical dependences of broadband overcast sky formulations, we have focused attention on the fundamental problem of single cloud decks over a nonreflecting surface. Three considerations are important for the development of accurate parameterizations, especially for the cloud heating rates. The first is the manner in which the broadband drop radiative properties are obtained. Methods that use arbitrarily defined mean single-scattering properties to obtain the broadband drop reflection and transmission can have errors in the cloud heating rates of 40% or more. A better approach appears to be to determine the drop reflection and transmission over the various spectral intervals, perform a spectral average to obtain the drop broadband values, and then convolve this with the broadband transmission function for the in-cloud vapor. The second factor is the dependence of the broadband drop reflection and transmission on the spectral irradiance at the cloud top. This implicitly brings in a dependence of the cloud radiative properties on the spectral attenuation by the water vapor above the cloud, with an increasing importance of this factor the lower the cloud top. By ignoring this dependence, a positive bias is introduced in the broadband drop absorption computation which implies an overestimate of the heating within the cloud. The third factor is the dependence of cloud absorption on the in-cloud vapor. Ignoring this effect leads to an underestimate in cloud heating, specifically for systems (especially extended ones) located in the lower troposphere (below ~600 mbar) where the vapor mixing ratios are high.

A parameterization is developed to account for the above- and the in-cloud vapor influences based on the ICRCCM drop models. It is tested for a range of overcast sky conditions. For the ICRCCM drop distributions, the relative error in the cloud heating rate is less than ~25% for the overhead sun case and less than ~30% for 75° incidence, with the larger relative errors occurring for thin, low-lying clouds (drop optical depths <2) and for geometrically thick, extended cloud systems that contain large amounts of water vapor.

Three other broadband treatments which have been used in or proposed for GCM studies, and that ignore one or more of the required considerations, are also studied. These three techniques, together with the method developed here, are intercompared using *Slingo*'s [1989] model of drop optical properties. The ranges in the values of the parameters directly affecting the overcast sky transfer, such as cloud drop radii, solar zenith angles, and systems containing varying amounts of water vapor and liquid water, are so vast that no single broadband scheme is able to yield highly accurate results for a variety of overcast sky conditions. In fact, it is possible to identify parameter spaces wherein each of the techniques proves superior in accuracy to all others. Neglecting the dependence of the cloud radiative properties on both the above-cloud and in-cloud vapor can lead to unacceptably large errors in the cloud heating rates (>50%). Ad-hoc enhancements in the in-cloud vapor absorption effect also can be poor because, for certain cases, the errors can again exceed 50%. If account is taken of the in-cloud vapor only, an interesting partial cancellation of errors occurs for extended cloud systems such that there is reasonable agreement with the reference results (errors <20%).

However, the same method yields larger errors (>35%) for systems <100 mbar thick, as well as for higher zenith angles. For the Slingo model, the parameterization developed here again has inaccuracies for extended clouds that contain large vapor amounts; however, for the range of overcast conditions explored, its overall accuracy remains better than ~30%.

In contrast to the sharp sensitivity to the above-cloud and the in-cloud vapor arising for the broadband computation of the absorbed fluxes in clouds, the relative errors in the reflected flux at the top of the atmosphere and the transmitted flux at the surface are not overly sensitive to the parameterization of either factor. In particular, the common assumption in GCMs that the cloud albedo is insensitive to the vapor inside the cloud appears to be a reasonable approximation. The maximum absolute errors for the fluxes at the atmospheric boundaries attain values of ~30 W/m^2 under the present broadband scheme, with the relative errors being less than ~15%. The absorbed fluxes in the noncloud layers of the atmosphere are less sensitive to the broadband methods.

While it is feasible to capture the effects of the above-cloud vapor in a broadband framework, the same is not true of the underestimate occurring in the in-cloud vapor effects. This deficiency persists for all broadband techniques studied here, although being masked in some instances owing to a fortuitous cancellation of errors. The multiple interactions occurring between drops and vapor at each frequency within the cloud, and the spectral integration of this effect may well be a complexity that cannot be expressed adequately by broadband concepts to a high degree of accuracy. Further, the prospect of combining the above- and in-cloud vapor effects into a general equation (similar to (21) and (22)) is not an encouraging one owing to intricate dependences on several factors.

In extending the broadband concept to arbitrary overcast atmospheres, there arise additional complexities in the treatment of vapor-drop radiative interactions. In particular, the spectrally dependent diffuse beam propagation and the multiple reflection of beams are not easy to account for in a general sense. There are cases involving multiple cloud decks (e.g., high cloud of moderate optical thickness overlying an optically thick low cloud) when the absolute and/or the relative errors in fluxes and heating rates with broadband parameterizations can exceed those stated above for single cloud decks.

The broadband overcast sky formulations prescribed here for the single (sections 5 and 6) and the multiple cloud deck (section 7) problems, together with the drop models of ICRCCM (CS or CL) or *Slingo* [1989] (e.g., the 4-band version), can be deployed in a climate or weather prediction GCM. On the basis of the analyses here, it is emphasized as a general rule that irrespective of the type of broadband parameterization employed, GCM investigations should consider carefully the domain and the magnitude of the potential errors due to the particular scheme. Although the use of the broadband concept in GCMs is appealing owing to their computational efficiency, there is a possible trade-off in accuracy which could become significant for certain applications.

An important conclusion from the present study is that even if one were to have the "correct" drop single-scattering properties and the "correct" vapor mixing ratios, the broadband radiative transfer concept for the vertically inhomogeneous overcast atmosphere, by its very nature, can lead to inaccuracies in the fluxes and the cloud heating rates. As an example, even if GCMs are able to compute drop reflection, transmission, and absorption accurately taking into account the spectral variations, errors could still arise due to the use of a broadband water vapor absorption scheme. While it remains to be seen whether broadband techniques can be improved further for arbitrary overcast atmospheres, it is likely that a highly precise treatment of solar interactions with vapor and drops may not be feasible with the present broadband approaches. Since errors in the overcast sky flux dispositions lead to biases in the diabatic heating estimates and the radiative drive of the atmosphere and are also an important component of cloud-climate interactions, more research is necessary for the development of accurate solar radiative parameterizations.

Acknowledgments. We thank J. D. Mahlman, S. Manabe, and M. D. Schwarzkopf, and two anonymous reviewers for their comments and suggestions on this manuscript.

REFERENCES

Charlock, T. P., and V. Ramanathan, The albedo field and cloud radiative forcing produced by a general circulation model with internally generated cloud optics, *J. Atmos. Sci.*, *42*, 1408–1429, 1985.

Chou, M.-D., and A. Arking, An efficient method for computing the absorption of solar radiation by water vapor, *J. Atmos. Sci.*, *38*, 798–807, 1981.

Chylek, P., V. Ramaswamy, and R. Cheng, Effect of graphitic carbon on the albedo of clouds, *J. Atmos. Sci.*, *21*, 3076–3084, 1984.

Coakley, J. A., R. D. Cess, and F. B. Yurevich, The effect of tropospheric aerosol on the Earth's radiation budget: A parameterization for climate models, *J. Atmos. Sci.*, *40*, 116–138, 1983.

Davies, R., W. L. Ridgway, and K.-E. Kim, Spectral absorption of solar radiation in cloudy atmospheres: A 20 cm^{-1} model, *J. Atmos. Sci.*, *41*, 2126–2137, 1984.

Fouquart, Y., B. Bonnel, and V. Ramaswamy, Intercomparing shortwave radiation codes for climate studies, *J. Geophys. Res.*, *96*, 8955–8968, 1991.

Fowle, F. E., The transparency of aqueous vapor, *Astrophys. J.*, *42*, 394–411, 1915.

Goody, R. M., and Y. L. Yung, *Atmospheric Radiation: Theoretical Basis*, 519 pp., Oxford University Press, New York, 1989.

Harshvardhan, R. Davies, D. A. Randall, and T. G. Corsetti, A fast radiation parameterization for atmospheric circulation models, *J. Geophys. Res.*, *92*, 1009–1016, 1987.

Joseph, J. H., W. Wiscombe, and J. A. Weinman, The delta-Eddington approximation for radiative flux transfer, *J. Atmos. Sci.*, *33*, 2452–2459, 1976.

King, M. D., and Harshvardhan, Comparative accuracy of selected multiple scattering approximations, *J. Atmos. Sci.*, *43*, 784–801, 1986.

Kratz, D. P., and R. D. Cess, Solar absorption by atmospheric water vapor: A comparison of radiation models, *Tellus, Ser. B*, *37*, 53–63, 1985.

Labs, D., and H. Neckel, Transformation on the absolute solar radiation data into the international temperature scale of 1968, *Solar Phys.*, *15*, 79–87, 1970.

Lacis, A. A., and J. E. Hansen, A parameterization of the absorption of solar radiation in the Earth's atmosphere, *J. Atmos. Sci.*, *31*, 118–133, 1974.

McClatchey, R. A., R. W. Fenn, J. E. A. Selby, F. E. Volz, and J. S. Garing, Optical properties of the Atmosphere, *Rep. AFCRL-72-0497*, 110 pp., Hanscom Air Force Base, Bedford, Mass., 1972.

Ramanathan, V., E. J. Pitcher, R. C. Malone, and M. L. Blackmon, The response of a GCM to refinements in radiative processes, *J. Atmos. Sci.*, *40*, 605–630, 1983.

Ramaswamy, V., and S. M. Freidenreich, Solar radiative line-by-line determination of water vapor absorption and water cloud extinction in inhomogeneous atmospheres, *J. Geophys. Res.*, *96*, 9133–9157, 1991.

Rothman, L. S., R. R. Gamache, A. Barbe, A. Goldman, J. R. Gillis, L. R. Brown, R. A. Toth, J. M. Flaud, and C. Camy-Perot, AFGL atmospheric absorption line parameter compilations: 1982 edition, *Appl. Opt.*, *22*, 2247–2256, 1983.

Sasamori, T., J. London,and D. V. Hoyt, Radiation budget of the southern hemisphere, *Meteorol. Monogr. 35*, pp. 9–23, 1972.

Slingo, A., A GCM parameterization of the shortwave radiative properties of water clouds, *J. Atmos. Sci.*, *46*, 1419–1427, 1989.

Stephens, G. L., S. Ackerman, and E. A. Smith, A shortwave radiation parameterization revised to improve cloud absorption, *J. Atmos. Sci.*, *41*, 687–690, 1984.

Wetherald, R. T., and S. Manabe, Cloud feedback processes in a general circulation model, *J. Atmos. Sci.*, *45*, 1397–1415, 1988.

Wiscombe, W. J., R. M. Welch, and W. D. Hall, The effects of very large drops on cloud absorption, I, Parcel models, *J. Atmos. Sci.*, *41*, 1336–1355, 1984.

Yamamoto, G., Direct absorption of solar radiation by atmospheric water vapor, carbon dioxide and molecular oxygen, *J. Atmos. Sci.*, *19*, 182–188, 1962.

S. M. Freidenreich, NOAA Geophysical Fluid Dynamics Laboratory, Princeton University, Princeton, NJ 08542.

V. Ramaswamy, Atmospheric and Ocean Sciences Program, Princeton University, Princeton, NJ 08542.

(Received July 31, 1991;
revised March 30, 1992;
accepted April 14, 1992.)